

BEAD GEOMETRY, MICROSTRUCTURE AND TEXTURE IN MULTI-AXIS
DIRECTED ENERGY DEPOSITION

A Thesis
Presented to
The Academic Faculty

by

Omar Hesham Elsayed

In Partial Fulfillment
of the Requirements for the Degree
Master of Science in the
George W. Woodruff School of Mechanical Engineering

Georgia Institute of Technology
[August 2020]

COPYRIGHT © 2020 BY OMAR ELSAYED

Bead Geometry, Microstructure and Texture in Multi-Axis Directed Energy Deposition

Approved by:

Dr. Christopher Saldana, Advisor
School of Mechanical Engineering
Georgia Institute of Technology

Dr. Thomas Kurfess, Co-Advisor
School of Mechanical Engineering
Georgia Institute of Technology

Dr. Katherine Fu
School of Mechanical Engineering
Georgia Institute of Technology

Date Approved: [07/20/2020]

[To my mom and dad.]

ACKNOWLEDGEMENTS

I would also like to first thank the Department of Energy for providing funding for this work via DE-EE0008303 without which this work would not have materialized. I also want to thank Mazak USA and Oak Ridge National Laboratories for providing me with the necessary equipment, expertise and supplies that were used in this study.

I would like to thank Dr. Christopher Saldana for his guidance and mentorship over the past 2 years. I also want to thank Dr. Thomas Kurfess and Dr. Katherine Fu for providing me with the necessary guidance, along with Dr. Saldana, to render this work a successful and fruitful addition to the scientific community. I want to especially thank Samuel Kersten, Myong Joon Kim, Derek Vaughan and Christopher Masuo for their invaluable help in conducting the necessary material deposition experiments for this study. I would also like to thank Materials Characterization Facility and the Montgomery Machining Mall for allowing me to use their shared user facilities to conduct some of my experiments. I want to thank Vinh Nguyen and Amey Vidvans for their help when it came to supply procurement and advice regarding metallography and some of the experiments conducted. Last, but not least, I want to thank my family and loved ones for believing me and cheering me on throughout.

TABLE OF CONTENTS

ACKNOWLEDGEMENTS	iv
LIST OF TABLES	vii
LIST OF FIGURES	viii
LIST OF SYMBOLS AND ABBREVIATIONS	ix
SUMMARY	x
CHAPTER 1. Introduction	1
1.1 Background	1
1.1.1 Hybrid Manufacturing – An Introduction	1
1.1.2 Hybrid Manufacturing Design & Process Planning – A Quick Overview	2
1.1.3 Additive vs. Subtractive Manufacturing – A Crossroads	3
1.1.4 Hybrid Manufacturing – An Alternative Approach	5
1.2 Motivation	5
1.3 Research Questions	7
1.4 Organization of Thesis	7
CHAPTER 2. Literature Review	9
2.1 Laser-Matter Interaction Phenomena – A Detailed Review	9
2.2 Research Gaps - Revisited	15
CHAPTER 3. Experimental Procedure	17
3.1 General Experimental Procedure & Simplifying Assumptions	17
3.2 Exp. 1 - Examination of Laser Incidence Angle Effects on Bead Morphology	20
3.3 Exp. 2 - Lead Angle Effects on Phase Composition & Texture	21
3.4 Exp. 3 - Lean & Lead (Pure & Compound) Angle Effects on Bead Microstructure	23
3.5 Exp. 4 - Laser Power Attenuation Quantitative Determination Study	26
CHAPTER 4. Results & Discussion	28
4.1 Results	28
4.1.1 Exp. 1 - Examination of Laser Incidence Angle Effects on Bead Morphology	28
4.1.2 Exp. 2 - Lead Angle Effects on Phase & Texture	29
4.1.3 Exp. 3 - Lean & Lead (Pure & Compound) Angle Effects on Bead Microstructure	32
4.1.4 Exp. 4 - Laser Power Attenuation Quantitative Determination Study	35
4.2 Discussion	36
4.2.1 Exp. 1 - Effect of Lead & Lean Angle on Bead Morphology	36
4.2.2 Exp. 2 - Lead Angle Effects on Phase & Texture	41

4.2.3 Exp. 3 - Lean & Lead (Pure & Compound) Angle Effects on Bead Microstructure	43
4.2.4 Exp. 4 - Laser Power Attenuation Quantitative Determination Study	44
CHAPTER 5. Study Limitations	46
CHAPTER 6. Study Conclusions	48
CHAPTER 7. Contribution & Implications of Study Findings	50
CHAPTER 8. Future Work & Next Steps	52
APPENDIX A. DETAILED MACHINE PARAMETERS	54
APPENDIX B. MICROGRAPH CLOSE-UPS	55
REFERENCES	61

LIST OF TABLES

Table 1	- 316L Austenitic Stainless-Steel Chemical Composition (wt%) (Sourced from LPW Technology Limited, a Carpenter Company)	16
Table 2	- AM Process Parameters	17
Table 3	- Examination of Laser Incidence Angle Effects on Bead Morphology – Examined Angular Configurations	19
Table 4	- Lean & Lead (Pure & Compound) Angle Effects on Bead Microstructure – Examined Angular Configurations	23
Table 5	- Laser Attenuation Quantitative Measurements – Examined Angular Configurations	26

LIST OF FIGURES

Figure 1	Typical hybrid manufacturing process chain	2
Figure 2	Orthogonal and non-orthogonal angle representations	5
Figure 3	Lead angle deposition techniques for acute and obtuse lead angle configurations	18
Figure 4	Laser incidence angle effects on bead morphology	20
Figure 5	X-Ray sample configurations	21
Figure 6	Lead angle effects on bead microstructure experimental setup	24
Figure 7	Lean and lead angle effects on bead morphology	27
Figure 8	X-Ray diffraction peak patterns	29
Figure 9	Orientation distribution function plots. $\Theta = 60^\circ$, $\beta = 0^\circ$	30
Figure 10	Orientation distribution function plots. $\Theta = 120^\circ$, $\beta = 0^\circ$	30
Figure 11	Orientation distribution function plots. $\Theta = 90^\circ$, $\beta = 0^\circ$	31
Figure 12	Pure lead, lean and compound angle effects on grain size across samples and sample regions	32
Figure 13	Micrographs of orthogonal and non-orthogonal solidification fronts	33
Figure 14	Laser attenuation quantitative measurements	35
Figure 15	Penetration depth changes due to employment of non-orthogonal angular configuration	36
Figure 16	Effect of deposition technique on powder catchment	38

LIST OF SYMBOLS AND ABBREVIATIONS

Θ	Lead Angle
β	Lean Angle
AM	Additive Manufacturing
ASTM	American Society for Testing & Materials
CAD	Computer Aided Design
CAM	Computer Aided Manufacturing
CW	Continuous Wave
DED	Directed Energy Deposition
FCC	Face Centered Cubic
GA	Gas Atomization
HAZ	Heat Affected Zone
ODF	Orientation Distribution Function
PBF	Powder Bed Fusion
PREP	Plasma Rotating Electrode Processing
PW	Pulsed Wave
SM	Subtractive Manufacturing
XRD	X-Ray Diffraction

SUMMARY

The purpose of this study is to examine the effect of varying laser incidence angles on textural, microstructural and geometric characteristics of DED-processed materials, provide a more comprehensive outlook on participating laser-matter interaction phenomena and ultimately devise strategies to ameliorate print performance. In this study, single-layer, single-/multi-track specimens were processed to examine the effect of non-orthogonal angular configurations on bead morphology, microstructure, phase composition and textural representation of DED-processed materials. Laser power measurements were also conducted to understand the effect(s) of laser spot size changes and laser attenuation on the effective power reaching the substrate surface. It has been observed that bead morphology experienced a normal curve behavior with increasing lead angles, while it experienced a decrease with decreasing lean angles. The orthogonal setting exhibited the most promising bead morphology values. An asymmetry in the distribution of the bead morphology plots indicates that there is preferential bias in utilizing a certain angular configuration over another in terms of potential incorporation of non-orthogonal deposition operations in industrial applications. No significant differences in phase composition, texture and microstructure were observed with processed samples of various angular configurations as well as raw, unprocessed powders, indicating that a potential route for enhanced process robustness is achievable without significantly affecting bulk material properties. In unfocused beams, laser incidence angles have little effect on the extent of laser power loss due to both laser spot size variations as well as powder cloud laser attenuation, indicating that more involved studies are required.

CHAPTER 1. INTRODUCTION

1.1 Background

1.1.1. Hybrid Manufacturing – An Introduction

Hybrid manufacturing is an emerging AM technology that incorporates both additive and subtractive manufacturing in producing net-shape components, yielding advantages that neither technology can supply when used in isolation [1]. Hybrid machines have AM capability alongside the tools used in multi-axis conventional machining. By combining additive and subtractive capabilities, components with impressive complex geometries can be manufactured and post-processed to produce dimensional accuracies and surface finishes that are unmatched by using current additive or subtractive technologies alone, all in one unified machine. One common AM technology typically employed in hybrid manufacturing is directed energy deposition (DED), which is intrinsically similar to laser cladding, a staple manufacturing process used regularly in industry. This manufacturing setup has become very popular in the aerospace industry. Turbine blade and other critical component repair has been proven to be viable with this technology, opening new avenues for research ventures and industrial applications [2]. In the race to render AM more commercially viable as a manufacturing process, hybrid manufacturing is a technology that is meant to bridge a disconnect between well established and emerging, state-of-the-art manufacturing technologies.

1.1.2. Hybrid Manufacturing Design & Process Planning – A Quick Overview

The design process for hybrid manufacturing is a highly involved, intrinsically iterative endeavor. Figure 1 illustrates a typical process chain for hybrid manufacturing [3]. First, the engineer must create the geometry using a CAD software. The design is then adjusted on dedicated 3D printing software such as Materialise Magics [4], or software tailored more towards hybrid manufacturing (i.e. HyperMill) to allow for successful printing without which the part will fail mid-build. This typically involves the selection and incorporation of support structures to hold the workpiece in place and maintain geometric stability due to the high residual stresses generated during the process. This becomes especially important in areas such as holes, channels and overhangs where geometric stability is at a minimum [5]. It also involves build orientation, which not only has an effect on the generated residual stresses and resultant print effectiveness, but also the component strength, surface roughness and dimensional accuracy of the print [6].

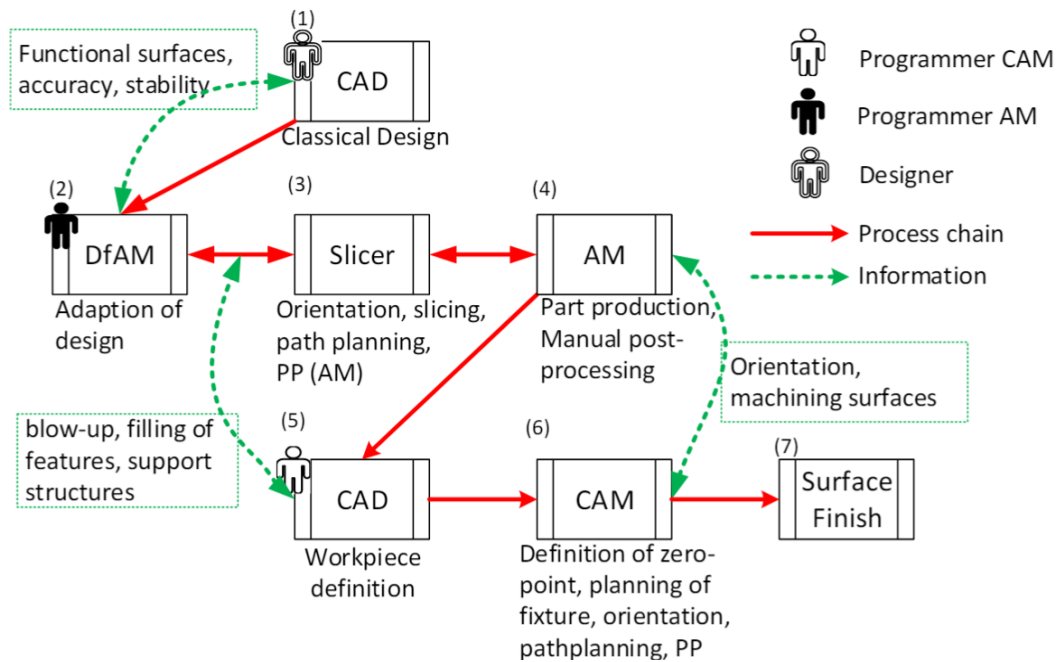


Figure 1. Typical hybrid manufacturing process chain [3].

Determining the proper process parameters is also key to ensuring the appropriate initial bulk and surface properties are produced to allow for accurate post-processing to be conducted (i.e. HIP treatment, surface finishing) [7]. An up-to-date awareness of the literature and organizational/industrial efforts (e.g. ASTM's F42 Committee on Additive Manufacturing Technologies [8]) is key to making sure that the most up-to-date and effective methods are used.

Once the component is successfully printed, the second iterative process of developing a CAM setup for subtractive manufacturing may begin. In this step, an experienced machinist can manually develop the machining process plan, or a CAM algorithm can be developed to conduct the automated CNC process. CAM software companies are developing increasingly easy-to-use interfaces that integrate the subtractive and the additive portions in CAM planning, such as HyperMill's Additive Manufacturing Suite [9]. This toolpath design step ensures the proper surface finish and dimensional accuracy are produced. Furthermore, the path plan needs to ensure that no tool-workpiece interference is involved that would result in inaccurate execution or, more critically, a tool crash. Most importantly, and what is considered most difficult here, is path planning to ensure proper tool-workpiece reachability, especially when targeting hard-to-reach process zones.

1.1.3. Additive vs. Subtractive Manufacturing – A Crossroads

Conventional subtractive manufacturing (SM) has experienced significant strides in recent years with the advent of multi-axis machining, especially when dealing with 5-axis machining freeform surfaces and complex geometries [10], which has become a well-established domain of manufacturing. The introduction of AM with SM to form hybrid manufacturing has, however, opened up a new realm of problems that is receiving significant interest from the scientific

community. Despite AM being especially celebrated for being capable of manufacturing highly complex geometries, it does have its limitations. Some of these limitations become highly apparent in hybrid manufacturing, where SM and AM reach a crossroads. More specifically, when dealing with highly intricate geometries in hybrid manufacturing, the issues that arise due to tool reachability and access in both additive and subtractive steps of the process become significant, increasing the probability of tool crashing dramatically. These matters become especially critical when engaging in repair operations, which are becoming increasingly popular and important in the aerospace industry [11]. With an already established base geometry, the subtractive and additive steps become highly spatially restricted, increasing the probability of tool inaccessibility or crashing. Thus, a creative approach to this problem must be devised to increase tool reachability and, consequently, process robustness.

In hybrid manufacturing, the status-quo setup involves incorporating a 5-axis subtractive machining configuration combined with a 3+2 axis additive manufacturing configuration. Examples of such a setup that are currently being used in industry can be observed in the Mazak VC-500AM [12], the DMG-MORI LaserTec 65-3D Hybrid System [13] and the Matsuura Lumex Avance-25 [14]. In a typical additive step in hybrid manufacturing, the printing involves having the laser head axis normal to the workpiece surface. This is typically the case due to the bulky nature of the deposition nozzles and their corresponding optics sub-systems commercially available today. Slimmer nozzle designs are currently being developed to address this issue but are still not yet commercially available [15].

1.1.4. Hybrid Manufacturing – An Alternative Approach

In an effort to tackle this problem domain, it is critical to understand the effects of non-orthogonal laser-workpiece configurations on printing performance in an effort to increase the freedom of motion during additive steps, thus improve tool reachability and enhance the robustness and effectiveness of the process. The angle between the laser head vertical axis and the workpiece surface is known as the laser incidence angle. In terms of deposition, there are two types of incidence angles: lead and lean. The lead angle is the angle produced in the YZ plane, while the lean angle (also known as the tilt angle [16]) is the angle produced in the XZ plane (assuming laser travels in the Y-direction). In general, there are 4 main configurations possible: orthogonal, pure lean/lead and compound lean/lead angles. Figure 2 visually illustrates the differences between the various angular configurations discussed here.

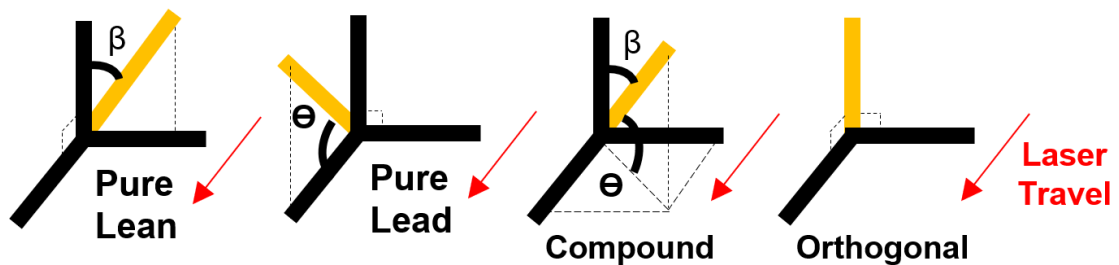


Figure 2. Orthogonal and non-orthogonal angle representations.

1.2 Motivation

In an effort to render hybrid manufacturing a more industrially viable option, significant research both within academia and industry is being conducted on devising strategies to increase the robustness of the technology. One approach that has been gaining increasing research interest is the utilization of non-conventional angular configurations, allowing for more elaborate toolpath

planning, increased freedom of motion and enhanced tool reachability, resulting in increased processing performance.

There have been various efforts to examine the effect of laser incidence angles on printing performance, including characteristics such as bead geometry and laser power/surface temperature distributions, amongst others. However, limited work has been conducted on examining the effect of pure lead/lean and/or compound laser incidence angles on bead texture and microstructure, respectively. Furthermore, no work has been done to relate such domains with bead geometry and laser attenuation or other participating physical phenomena to provide a more holistic understanding of some of the underlying laser-matter interaction phenomena at play in directed energy deposition processes. From an industrial standpoint, understanding the effects of utilizing non-orthogonal setups can provide an important avenue for increasing the freedom of toolpath planning, therefore increasing the robustness of the process and allowing for certain, previously unfeasible process plans to be undertaken with more confidence and capability. The purpose of this study is thus three-fold, and involves:

1. Examining the effect of varying laser incidence angles on geometrical, microstructural and textural characteristics of DED-processed materials.
2. Developing a better understanding of laser-matter interaction phenomena present in DED-AM processes.
3. Devising strategies to increase processing efficiency, quality and robustness to reduce print lead times and/or energy requirements.

The ultimate goal of this new research effort is to understand the effect that participating phenomena have on the structure and properties of the printed material when using non-orthogonal

configurations. By developing an accurate understanding of such phenomena, the ability to produce consistent geometries, structures and properties, agnostic of the angular configuration, can be realized. Thus, this will render the hybrid manufacturing process more robust and attractive for industrial applications.

1.3 Research Questions

There are multiple research questions at hand in this study, which are motivated by the gap in the extant literature. The over-arching goal of this work is to attempt at answering these questions in a fashion that would shed light on how certain phenomena behave in these simulated, controlled circumstances. More specifically, this study aims at answering the following questions:

1. What morphological changes can be observed in a deposited bead when employing various, non-orthogonal laser incidence angles?
2. Does the phase composition and resultant texture demographic change with varying laser incidence angles?
3. What microstructural changes occur when varying laser incidence angles?
4. What differences in absorbed power can be observed by varying the laser incidence angle configurations? Can the observed differences provide an explanation and/or decouple power losses due to laser attenuation vs. those due to laser spot size and shape variability?

1.4 Organization of Thesis

This manuscript is divided into six chapters. The first chapter discussed the general background regarding hybrid manufacturing and the motivation/relevance of this study. The second chapter brings the reader up to speed with the relevant literature and the present research

gaps that this study plans on filling. The third chapter focuses on detailing the various experiments conducted in this study. The first experiment focuses on examining the effects of the various combinations of lead and lean angles on bead geometry, which included penetration depth, bead height and bead width. The second experiment involves comparing the phase composition and textural representations of orthogonal and pure lead configurations with the raw, unprocessed powders via XRD measurements conducted on single-layer, multi-track samples. In the third experiment, a more detailed approach of non-orthogonal angles is examined by processing single-layer, single-track specimens of various lead angles, lean and compound angles (along with orthogonal setup), where the bead microstructure was compared both within various regions of a bead and across similar regions in beads of varying angular configurations. The fourth and final experiment involves a laser power measurement experiment that was conducted to examine the effects of non-orthogonal angular configurations on the extent of power loss with the powder feed on and off, in an effort to decouple the effects of spot size variations and laser attenuation due to powder cloud formations. The fourth chapter of this manuscript exhibits the obtained results as well as discussion of these results. The fifth chapter provides a brief overview of the study limitations, while the sixth chapter summarizes the general conclusions of the study. Finally, the seventh and eighth chapters examine the main contributions/implications of the work done, as well as what would constitute a sensible set of future work endeavors that would most logically flow with this study, respectively.

CHAPTER 2. LITERATURE REVIEW

2.1 Laser-Matter Interaction Phenomena – A Detailed Review

There is extensive research being conducted to examine the multiple physical phenomena at play when it comes to material deposition in hybrid manufacturing in general, which include laser-matter interactions [17], solidification dynamics [18] and microstructural evolution [19], to name a few. For the mass commercialization of AM to be realizable, it is important to determine what manufacturing conditions will yield the most appropriate material characteristics and properties to fit the applications in question, and ultimately allow for higher performing, better quality products to be produced more cheaply and more reliably.

A critical element of AM is the powder particles used during manufacturing. Extensive research has been conducted on characterizing the effects of processing method, chemical composition, powder particle size and morphology on printing performance in AM [20]. This becomes especially important in directed energy deposition where, as compared to powder bed fusion (where the powder is relatively static), powder motion adds to the complexity of the process. Particle composition, size and size distribution were observed to have one of the most significant effects on printing quality and resultant material properties. Kakinuma et. al. examined the effect of powder size, distribution, and composition on the generation of structural defects, including compositional variations and void density, in the directed energy deposition processing of Inconel 625 [21]. They found that a smaller particle size and a narrower particle size distribution reduces the probability of void and crack generation, which in turn increases the tensile strength of the deposited material. They also observed that the presence of carbon can facilitate void generation.

In an effort to enhance particle composition integrity as well as reduce particle size and size distribution, the manufacturing processes used to produce such powders plays a critical role in how these powders perform when ultimately used in deposition operations. Ahsan et. al. performed a comparative study between gas-atomized (GA) and plasma rotating electrode (PREP) processed powders on the directed energy deposition performance of Ti-6Al-4V [22]. It was observed that PREP-processed powders resulted in lower intralayer porosity, an enhanced surface finish and a higher deposition rate capability. However, the microstructural evolution of both types of powders was observed to be equivalent, exhibiting an $\alpha + \beta$ general microstructure that is epitaxial and non-martensitic in nature. Zhong et. al. performed a similar study where they examined the differences between PREP and GA-processed powders on porosity and microstructure in Inconel 718 [23]. As observed with Ahsan et. al.'s study, porosity and dilution extent were lower in PREP-processed powder samples than in GA-processed samples. However, GA-processed samples experienced smaller dendrite arm spacings, lower Laves phase volume fractions and Nb segregation. It has been argued that these observations are due to the higher gas volume fractions inherently present due to the nature of GA powders, therefore resulting in elevated cooling rates (and thus enhanced microstructures). Mahmood et. al. examined the differences between 316L GA-powders and metal shavings of a similar size range on printing effectiveness [24]. Metal shavings resulted in improved deposition as well as diminished gas porosity when compared with the atomized powders. However, due to the higher prevalence of oxides on the metal shavings, higher surface oxidation was also observed.

Laser-matter interactions also play a critical role in the printing performance in directed energy deposition, as well as other additive manufacturing methods. Depending on what AM process is being utilized (i.e. DED vs. PBF), the cooling and solidification phenomena involved

are directly affected by the interplay between particle structure/morphology, absorbed power, beam velocity, and substrate preheating conditions (if any), amongst many other process parameters [25]. As a result, depending on the thermal histories and surrounding volumes (i.e. deposition near edges, in the middle of the substrate, or on top of previous layers), the produced microstructure, texture and resultant residual stresses can differ dramatically [26]. The interplay between the powder characteristics, flow parameters, ambient conditions and laser features involved thus govern the resultant deposition performance.

Within the scientific and industrial communities, significant interest is directed towards understanding the effects of laser parameters and characteristics on resultant printed material properties. For instance, Ravi et. al. compared the effects of continuous wave (CW) vs. continuous wave + pulsed wave laser (CW+PW) modes on microstructural evolution in PREP-processed Ti-6Al-4V deposited samples [27]. They found that the CW mode facilitated large columnar grain growth to occur. However, the CW+PW mode encouraged finer, more equiaxed grain growth while inhibiting epitaxial grain growth. The laser modes had no perceivable differences on phase composition. Higher laser power, on the other hand, was observed to yield coarser grains and induce phase transformations. Such phase changes involve the transformation from fine martensitic and α phase microstructures to larger lamellar $\alpha+\beta$ microstructures with an increase in power. In another effort to further understand the effects of laser-matter interactions on printing performance, Kobryn et. al. examined the effect of laser scanning speed on structural and geometric characteristics Ti-6Al-4V deposited samples [29]. The presence of lack-of-fusion and gas pore defects increased with a higher scanning speed, as well as a higher laser power. Deposition height also decreased with increasing scanning speed, while the effect of power on height was not

clear. Furthermore, columnar grain width increases with increasing scanning speed as the cooling rates increase. Substrate thickness did not have a direct effect on columnar grain width, though.

In order to provide a holistic view of laser-matter interactions of this process, research has been conducted to examine the powder particle's kinematic role in printing performance. Costello et al. performed a parametric study of DED-processed 316L samples to examine effect of powder feed rate (amongst other parameters) on the mechanical and microstructural properties of the deposited material [28]. They conjectured that a higher powder feed rate can result in insufficient/incomplete particle melting due to the reduced interaction time between the laser and the powder particles. Such partially melted particles can play a direct role in more pronounced component brittleness. Furthermore, the microstructure of such particles is equivalent to the raw powders. Cellular structures with various orientations were also observed, along with dendrite formations, possibly due to remelting. Large gradients in cooling rates also resulted in some delta-ferrite phase structures to appear, which are primarily affected by cooling rates and elemental segregation that may occur.

In order to prevent excessive high-temperature oxidation during deposition, hybrid manufacturing typically involves the incorporation of shielding and carrier gases, typically composed of argon, to inhibit oxidation formation during printing, and thus prevent detrimental effects from manifesting in the printed product. The integration of such gases adds to the complexity of the process, and thus attracts much interest from various research groups within the field. For instance, Ruiz et. al. studied the role shielding gas compositions play in the deposition of Inconel 718, where they examined their effects on melt-pool temperatures and bead morphology [30]. They used various combinations of argon and helium gas mixtures to perform their study. They found that clad height decreases with an increase in He, while the remainder of the bead

features did not change significantly. Helium was also observed to encourage higher melt-pool temperatures, resulting in lower wet angles (which can explain the reduced bead height). In another effort, Eo et. al. investigated the effect of shielding gas flow rates on inclusion characteristics involved in the directed energy deposition of 316L samples [31]. Oxygen presence within the melt-pool was observed to decrease with increasing shielding gas flow rates. In turn, a reduction in oxygen presence can affect melt pool surface tension in a way to possibly allow for a reversed Marangoni flow. Furthermore, lowering the gas flow rate while raising the laser power resulted in the formation of coalescence of smaller inclusions to form larger inclusions (over 10 μ m), which are detrimental to tensile strength.

In directed energy deposition, a conically shaped nozzle outputs powder with an angle that allows the powder particles to meet the focused laser beam at the workpiece surface. During deposition, however, not all the deposited powder is melted and subsequently bonded to the surface, resulting in inhibited powder catchment efficiency. The interactions with the shielding and carrier gases can exacerbate this situation as well. The rather random and turbulent rebounding of the powder particles away the workpiece surface results in a powder cloud to form. This powder cloud thus results in unwanted laser-powder interactions that occur as the particles are flying away from the workpiece. As the particles get exposed to the laser beam, they absorb and/or reflect some of the laser energy. As a result, the effective laser energy reaching the workpiece surface (and consequently used to create the melt pool) is lower than the intended laser energy that left the laser beam source. This is referred to as laser attenuation and can result in considerable efficiency losses during deposition.

Laser attenuation is, in principle, the loss of a laser beam's effective optical power due to the simultaneous development of a partially absorbent and/or reflective medium along the laser

beam's path as deposition occurs [32]. In additive manufacturing, this optical obstruction manifests in the form of the aforementioned non-melted powder particle cloud [33] and vapor plumes [34] (more prevalent in low-melting and boiling point alloys) that form during the deposition process. As this absorbent/reflective medium obstructs the laser beam path, some power is lost and/or dissipated en-route, resulting in power losses that can mount up to 50% in focused beams vs. non-focused beams [32].

The laser incidence angle can have a direct effect on the extent of laser attenuation and can be strategically employed to reduce efficiency losses that are endemic of more extreme process parameters. Various theoretical models have been developed and coupled with experimental validation to analyze the effects laser attenuation has on deposition performance and have coupled their results with experimental data as a validation front. For instance, Fu et. al. developed a theoretical model that analyzes the effect of stream speed, powder particle deposition rates and laser incidence angles on resultant laser power and surface temperature distribution [35]. It was observed that lower angles resulted in more asymmetric particle temperature distributions as well as lower average temperatures due to the reduced travel experienced by the particles within the laser field. It was also observed that laser attenuation increased with increasing angles, resulting in upwards of 50% effective power losses and transforming the power distribution from Gaussian to non-Gaussian in nature. Liu et. al have also theoretically and experimentally shown that laser attenuation is directly linked to particle feed rate and particle speed, with up to 10% efficiency losses in conventional process parameter adjustments [36]. Pinkerton et. al. developed an analytical model that quantitatively predicts the extent of laser attenuation and resultant powder temperatures below the laser nozzle [37]. They found that laser attenuation becomes significantly more pronounced once the annular powder streams converge to form a single stream at the center,

though is not zero beforehand. They also observed that the powder temperature reaches a maximum average at the center of the stream.

The laser incidence angle can also have a direct effect on the resultant print bead morphologies, which significantly affect process planning in the hybrid manufacturing realm. For instance, Hao et. al examined the effect of lean/tilt angle between the laser nozzle and substrate on bead geometry in various configurations, which include an orthogonal setup, a tilted nozzle, tilted nozzle and substrate, and a tilted substrate (the more common convention used in industry today) [16]. They observed that an increasing tilt angle results in an increasing clad width and peak point shifting, regardless of the configuration. This was attributed to the presence of gravitational effects and/or changes in spot size and geometry, depending on whether the substrate or the nozzle is tilted, respectively.

2.2 Research Gaps - Revisited

As previously discussed, much work has been conducted on examining the effects of various laser-matter interactions on printing performance in hybrid manufacturing. However, little research has been conducted on understanding the effects of employing non-orthogonal angular configurations in deposition operations on printing performance, namely laser power and temperature distributions and bead morphology. Furthermore, no research has been conducted on examining the effects of non-orthogonal angular configurations on microstructure and textural representation, nor has there been any effort in developing a correlation of such characteristics with bead morphology.

This work is aimed at targeting these specific topics to develop a more thorough understanding of how employing non-conventional deposition techniques alters the laser-matter

interaction phenomena present in hybrid manufacturing. In an effort to bring this technology closer to becoming a highly competitive manufacturing technique, increasing the robustness of the process by devising strategies to increase the freedom of motion of the equipment is a logical step forward in that direction.

CHAPTER 3. EXPERIMENTAL PROCEDURE

3.1 General Experimental Procedure & Simplifying Assumptions

Directed energy deposition (DED) was employed to perform the required experiments in this study using the Mazak VC-500AM HWD hybrid machine. The powder material of choice was 316L austenitic stainless steel (sourced from LPW Technology Limited, a Carpenter Company) which is of considerable interest in the AM academic and industrial research communities. The material was deposited on a 316L substrate with a thickness of 0.25in to prevent excessive distortion/bowing endemic of the high temperatures and cooling rates (thus resultant residual stresses) experienced in the process. This thickness also provided enough heat sinking capabilities to the deposited material, thus mimicking those typically observed in industrial applications that involve thick-wall substrate structures. The chemical composition of the powder material is provided in Table 1. The particle size distribution of the powder used in this study was within 45-106 μ m, per the sieve analysis conducted following ASTM-B214. The process parameters were kept constant to isolate effects of incidence angle on phase composition, texture, bead morphology and microstructure. Table 2 illustrates the parameters used for this process.

Table 1. 316L Austenitic Stainless-Steel Chemical Composition (wt %) (Sourced from LPW Technology Limited, a Carpenter Company)

Fe	Cr	Ni	Mo	Mn	Si	N	C	Cu	O	P	S
Bal.	17.8	13.0	2.40	1.04	0.64	0.1	0.02	0.02	0.01	0.01	0.004

Table 2. AM Process Parameters

Parameter	Value
Scanning Speed (mm/min)	300
Laser Power (W)	400
Nozzle Gas Flowrate (L/min)	2
Shielding Gas Flowrate (L/min)	10
Carrier Gas Flowrate (L/min)	5
Metering Disc Duty Cycle (%)	66

As discussed previously, a total of 4 experiments were conducted in this study. In the first experiment, the pure lead and pure lean angle configurations effects on bead morphology were examined to better understand the inherent limitations in this unique processing technique, and whether alternative deposition techniques can be used to enhance the robustness of the hybrid manufacturing process. The second experiment focused on determining differences in phase composition and texture between non-orthogonally (pure lead) deposited, material, orthogonally deposited material, and the raw, unprocessed powder. In the third experiment, pure lead, pure lean and compound angle configurations and their effects on microstructure were examined. Finally, laser power measurements were conducted using a laser power meter to examine how the effective power reaching the supposed substrate is affected by the usage of non-orthogonal incidence angles, both with the powder feed on and off, in an attempt to decouple laser spot size and laser attenuation effects.

Due to the 3+2 axial configuration that the additive deposition head possesses, there are 2 deposition techniques with regards to lead angle. For angles lower than 90°, the deposition head ‘climbs up’ the substrate, as shown. For angles larger than 90°, the deposition head ‘climbs down’ the substrate. Figure 3 illustrates the 2 deposition techniques discussed.

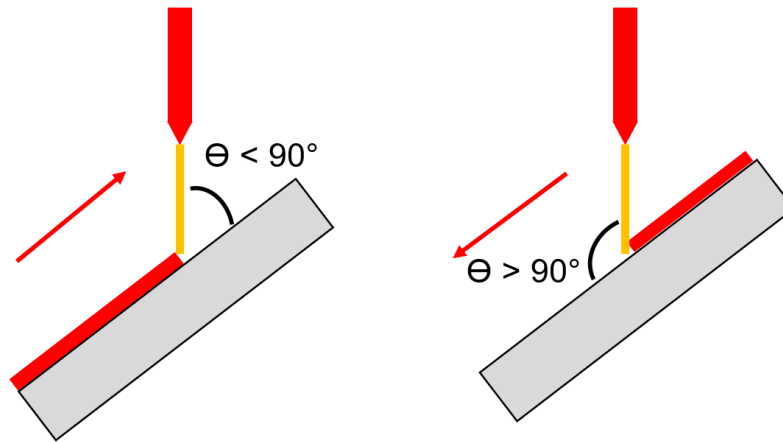


Figure 3. Lead angle deposition techniques for acute and obtuse lead angle configurations.

In this study, some assumptions were made to restrict the complexity of the problem being targeted:

1. Controllable process parameters (i.e. laser power, powder feed rate...etc...) remain constant throughout the entirety of a deposition or laser measurement event.
2. The ambient conditions remain constant throughout a deposition or laser measurement event, including ambient temperature and humidity.
3. Laser incidence angle variations observed throughout a deposition or laser power measurement event are assumed to be minute and have negligible effects on print quality.
4. The slight bowing/distortion experienced by the substrate during deposition is small enough to not result in any changes in the extrinsic and intrinsic characteristics of the deposited samples.
5. Satellite bead formations typically found along the outskirts of the primary bead are ignored in metallographic examinations.

3.2 Experiment 1 - Examination of Laser Incidence Angle Effects on Bead Morphology

In this experiment, a set of 5” long single tracks were deposited of the orthogonal, pure lean and pure lead angular configurations. The angular configurations examined here are illustrated in Table 3. Long tracks were deposited in this experiment to produce up to 5 cross sectional samples for each condition to ensure statistical significance and reproducibility. The samples were deposited approximately 5mm apart in order to prevent heat-affected zone (HAZ) overlap, which can interfere with the melt-pool and solidification dynamics as well as the resultant microstructure of the deposits. A single layer track was employed to avoid altering melt-pool behaviors and introducing secondary effects of vertical inter-layer diffusion and solidification phenomena, therefore convoluting the primary results of this study. A total of 9 different angular configurations were examined, including orthogonal, pure lean, pure lead setups.

Table 3. Experiment 1 Examined Angular Configurations

Angular Configuration	Lead Angle - Θ (°)	Lean Angle – β (°)
Orthogonal	90	0
Pure Lean	90	15, 30
Pure Lead	45, 60, 75, 105, 120, 135	0

After deposition, the samples were sectioned and prepared for metallographic analysis. The samples were cold mounted in curable epoxy resin and subsequently polished down to 0.05 μ m for a flat, scratch free finish. They were then etched with a 3:2:1 solution of distilled water, hydrochloric acid and nitric acid, respectively, to allow for accurate bead geometry appearance and subsequent examination using a Leica LASX optical microscope. Bead height, width and penetration depth were measured using Leica’s LASX analysis software and henceforth recorded. The goal of this experiment was to examine the lean and lead angle effects on bead morphology as compared to the orthogonal condition. Figure 4 illustrates the experimental and metallographic analysis setups.

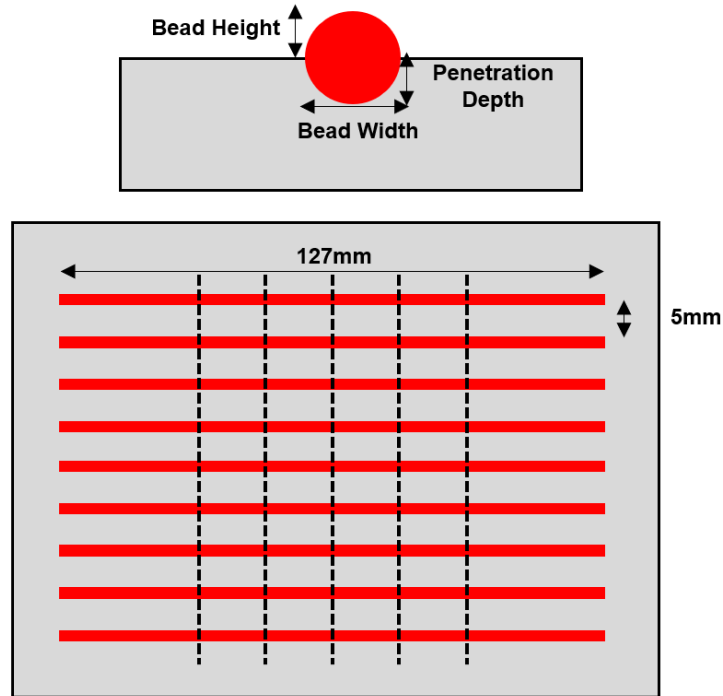


Figure 4. Laser incidence angle effects on bead morphology - Experimental setup. Top: cross sectional display of analysis area. Bottom: Overall experimental setup, with the dashed lines representing the sectioning lines.

3.3 Experiment 2 – Lead Angle Effects on Phase Composition & Texture

In this experiment, samples were prepared to examine the effects of lead angles on phase composition and texture representation in deposited tracks. Three 1”x 0.5”, single-layer, multi-track samples were produced: a sample with an orthogonal configuration two samples with pure lead angles of $\Theta = 60^\circ$ and 120° . A single layer track was employed to avoid altering melt-pool behaviors and introducing secondary effects of vertical inter-layer diffusion and solidification phenomena, therefore convoluting the primary results of this study. Figure 5 illustrates the main angular configurations and sample dimensions used in this study.

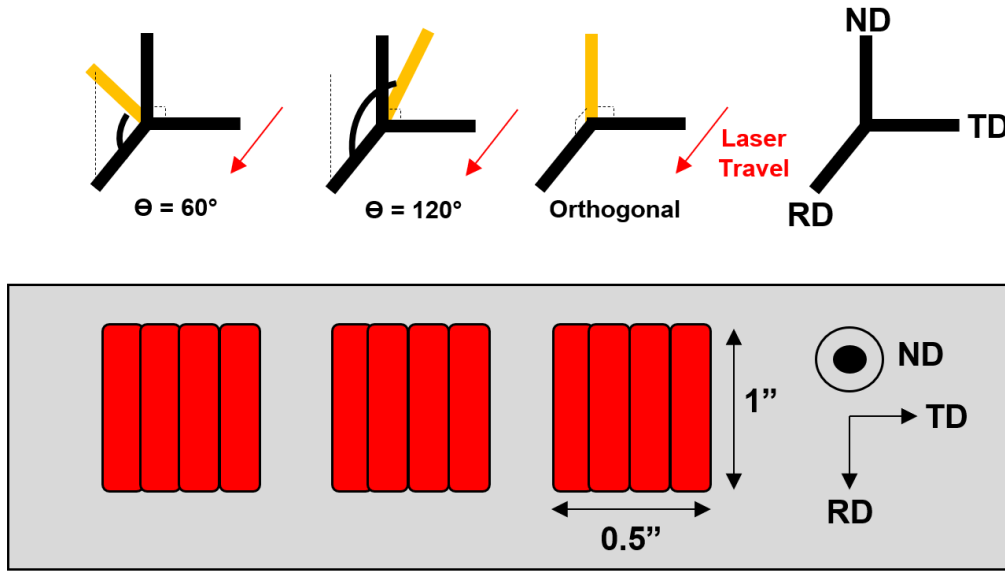


Figure 5. X-Ray sample configurations. Bottom left: $\Theta = 60^\circ$ pure lead condition. Bottom middle: $\Theta = 120^\circ$ pure lead condition. Bottom right: Orthogonal condition. Rolling direction (RD) represents the laser travel direction. The normal direction (ND) represents the vertical axis.

After deposition, the samples were polished down to 4,000 grit in preparation for the X-ray diffraction measurements. For this study, two X-ray machines were used: the Panalytical Empyrean XRD System for phase analysis (using a Chi-Phi-Z stage and a Cu anode material) and the Panalytical XPert PRO MRD XRD system for textural analysis. The generator voltage and tube current were kept at 45kV and 40mA throughout all measurements on both machines.

The phase analysis was conducted on all three samples as well as the raw, unprocessed powder to provide a comparative basis on the processing effects on phase composition. The X-Ray scan range was between 30° and 140° with a Continuous scan setting. The Empyrean machine was used here. A more comprehensive list of the exact measurement parameters used for the measurements conducted in this study is provided in Tables A1 in the Appendix.

The textural analysis was conducted to obtain orientation distribution functions (ODF) to map the textural demographics present in the samples. The orientation distribution functions provide a global representation of texture within a large area of a sample, thus providing a more high-level view of the texture demographics in the investigated samples. The coordinate transformation angles φ , φ_1 and φ_2 represent the 3 angular transformations required to convert from the sample's coordinate system to each crystal plane's coordinate system within the sample. A high intensity observed in an ODF plot indicates that there is a high prevalence of a certain crystal plane with the prescribed crystallographic orientations represented by the φ , φ_1 and φ_2 . In other words, words, these angular combinations represent the crystallographic orientations present within the samples.

The MRD system was utilized for this experiment. In terms of incident beam optics, the MRD machine is equipped with an 8mm polycapillary lens, coupled with a 2x2 masking lens. For the diffracted beam optics, the machine was equipped with a 0.27° parallel plate collimator and a proportional detector. The resultant raw data was then corrected for background noise and normalized to obtain the accurate ODF representations. Once the measurements were completed, Panalytical HighScore Plus® was used to analyze the diffraction peak patterns for materials/phase identification. Textural data was analyzed using the MATLAB MTEX toolkit. More specifically, MTEX was used to produce the required orientation distribution functions for data visualization of a global map of texture within each sample. The raw data was corrected for background noise and normalized prior to all calculations to render more meaningful results.

3.4 Experiment 3 – Lean & Lead (Pure & Compound) Angle Effects on Bead Microstructure

In this experiment, the bead microstructure of pure lead, pure lean, compound lead/lean and orthogonal configurations was examined and henceforth compared. A set of 1” single-track,

single-layer samples with various angular configurations were deposited. The specific angular configurations are illustrated in Table 4. The samples were deposited approximately 5mm apart to prevent HAZ overlap. They were then sectioned and polished down to 0.05 μ m for a flat, scratch-free mirror finish. The samples were then etched using the same etching solution described in Experiment 1 to allow for accurate microstructure and metallographic examination using the Leica LASX optical microscope. In this experiment, the microstructure was carefully analyzed. Figure 4 illustrates the sample setups examined here, as well as the strategy used to examine the microstructure.

Table 4. Experiment 3 Examined Angular Configurations

Angular Configuration	Lead Angle - Θ ($^{\circ}$)	Lean Angle - β ($^{\circ}$)
Orthogonal	90	0
Pure Lean	90	15
Pure Lead	75, 105	0
Compound	75, 105	15

The grain size was examined in 7 regions that cover the entirety of the bead: center, bottom-left, bottom-center, bottom-right, left, top-center and top-right. The examined regions were 100 μ m x 100 μ m squares, as illustrated by the green boxes in Figure 6. The conventional, line-intercept manual method was employed here. Five straight, horizontal lines were drawn at equal intervals within the square region. To determine the grain size, the number of grain boundaries present along the 100 μ m drawn line were counted, and Equation 1 [38] was used to calculate the effective grain size:

$$Grain\ Size = \frac{Number\ of\ Grain\ Boundaries}{Line\ Length} \quad (1)$$

After obtaining the grain sizes in the respective regions, the data was plotted to compare grain size values/demographics using two approaches:

1. Compare the grain sizes between regions within a single bead to develop an understanding of the inter-bead grain size demographic and use that as a precursor for comparing between beads.
2. Compare the grain sizes of specific regions between different beads to determine if different angular configurations result in altered microstructure in the same regions of a bead.

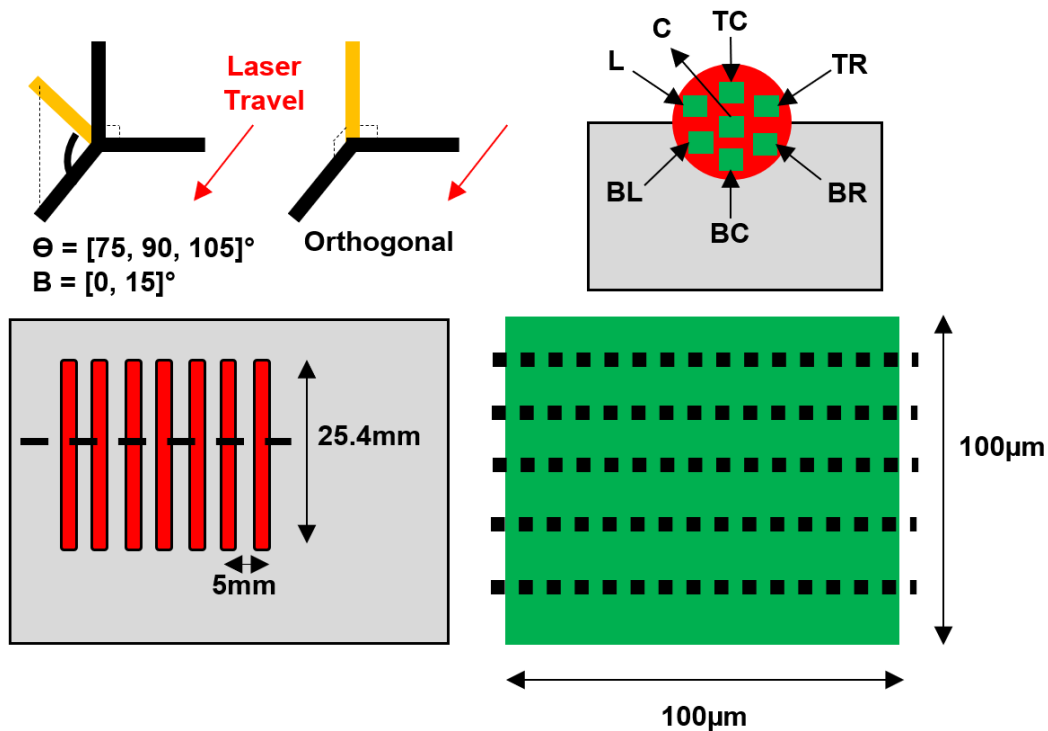


Figure 6. Lead angle effects on bead microstructure experimental setup. Top left: Angular configurations. Bottom left: Top view of single-track setup on substrate, along with the sectioning line. Top right: Cross sectional area to be investigated metallographically. L = left, C = center, TC = top center, TR = top right, BL = bottom left, BC = bottom center, BR = bottom right. Bottom right: examined region manual intercept method setup.

3.5 Experiment 4 – Laser Power Attenuation Quantitative Determination Study

In this experiment, a laser power meter was utilized to quantitatively measure the effective power reaching the surface of a substrate under controlled conditions. The power absorbed by the power meter (termed the effective power here) was then compared to the command power (which was set at 400W for this experiment) to obtain the difference in power, which would represent the power loss experienced as the laser travels to the substrate. Equation 2 represents this simple calculation.

$$P_{effective} = P_{command} - P_{attenuated} \quad (2)$$

A Macken Instruments P-2000Y Analog Laser Power Probe (2,000W Rating) was used in this experiment. The analog power probe was fixtured into the hybrid machine bay and was exposed to the laser at a 33mm stand-off distance that produces a laser spot size slightly larger than the 1.09cm minimum spot size recommended by the manufacturer. The power probe was then exposed to the laser for approximately 21s to prevent damage to the equipment as well as ensure an accurate reading was conducted, as per the device manufacturer instructions. Due to the cylindrical shape of the power probe, the laser travel path was adjusted to form a circular trajectory at an angular speed equivalent to the 300mm/min linear speed employed in previous experiments in this study. The diameter of this path was also adjusted to allow for a full 360° turn within the allotted 21s exposure time. This would ensure that the probe was adequately and uniformly exposed to the laser, thus facilitate proper laser absorption and accurate data collection.

Once this was complete, the power meter was left idle to allow for the readout dial to reach an equilibrium and the resultant equilibrium value was then recorded. This process was repeated

for all the angular configurations to be examined here. In between runs, the power meter was cooled down to room temperature by submerging it in water and ensuring it has reached ambient temperature. This was done by keeping the probe submerged under water until the dial has successful reached the 0W reading. Once the dial reached 0W, the probe was then adequately dried to ensure no moisture was left on the probe surface, which can lead to inaccurate readings. Table 5 represents the examined angular configurations. The goal here was to attempt to decouple the effects of the laser attenuation and laser spot size/shape on the laser-particle interactions during deposition, and thus isolate the phenomena in terms of their potential participation in the observed bead morphology of the samples.

The measurements were first conducted with the powder feed turned off to examine the effect of laser spot size and shape on the effective power reaching the surface. Afterwards, the measurements were conducted with the powder feed on to determine the effect of the resultant powder cloud on the effective power. Some preliminary runs of this experiments illustrated that the current process parameters and the preset 33mm standoff distance did not cause any damage to the probe surface, which can be detrimental to the calibration of the device. The preliminary runs were also conducted to ensure that no powder is being deposited directly on the probe, which can lead to complications in data collection.

Table 5. Experiment 4 Examined Angular Configurations

Angular Configuration	Lead Angle - Θ (°)	Lean Angle - β (°)
Orthogonal	90	0
Pure Lean	90	15, 30, 45
Pure Lead	45, 60, 75, 105, 120, 135	0
Compound	45, 60, 75, 105, 120, 135	15, 30, 45

CHAPTER 4. RESULTS & DISCUSSION

4.1 Results

4.1.1 Experiment 1 – Effect of Lead & Lean Angle on Bead Morphology

Figure 7 illustrates the resultant bead widths, heights and penetration depths of the various angular configurations examined. For the pure lean angle configurations, it can be observed that all bead morphology parameters experienced a consistent, gradual drop in value with increasing lead angle as compared to the orthogonal condition. More specifically, the penetration depth, bead height and bead width dropped by approximately 50%, 30% and 10% as the lead angle increased from 0° to 30° , respectively.

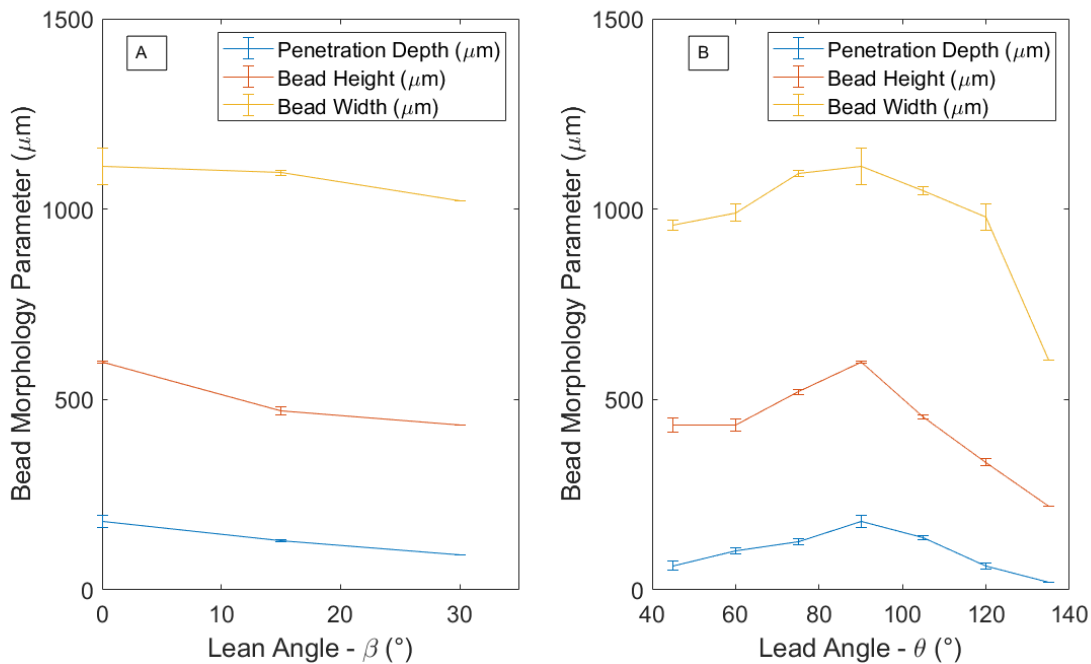


Figure 7. Lean and lead angles effects on bead morphology. [A] Pure lean angular configurations. [B] Pure lead angular configurations.

With regards to the pure lead angular configurations, the orthogonal condition exhibited the largest morphology parameters as compared to the other, pure lead conditions. A normal curve behavior was observed in all 3 parameters. However, there was an observed asymmetry in the curves. Bead morphology parameters were lower in lead angle configurations higher than 90° as compared to their mirror equivalents (i.e. 75° vs. 105° , 60° vs. 120° , 45° vs. 135°). However, the penetration depth at 75° and 105° were observed to be slightly more equivalent here, with the 75° condition being $\sim 7\%$ larger than the 105° condition. Nevertheless, more extreme angular configurations experienced greater disparity when compared with their mirror counterparts.

4.1.2 Experiment 2 – Lead Angle Effects on Phase & Texture

Figure 8 illustrates the X-Ray diffraction peaks of the non-orthogonal and orthogonal configurations as well as that of the unprocessed powders. The diffraction peaks were overlaid on top of each for ease of visualization. The material candidates that matched the unprocessed and processed samples (C-Cr-Fe-Ni and $\text{CFe}_{15.1}$) were austenitic FCC phases. Despite the peak patterns being slightly off the expected γ -Fe austenitic phase, the qualitative determination of an austenitic FCC phase was sufficient for subsequent analyses, which were highly dependent on the h-k-l values representative of the detected peaks at lower angles.

Figures 9 to 11 illustrate the calculated orientation distribution functions of the non-orthogonal and orthogonal processed samples. From the texture measurements conducted, it was observed that similar textural representations were present in orthogonal and non-orthogonal samples. Significant texture was observed at $\varphi = 60^\circ$, $\varphi_2 = 45^\circ$ and all φ_1 values for all the samples, indicating that fiber texture is dominant in this specific orientation. Furthermore, high texture intensities were observed in the $\varphi_2 = 15^\circ$ and $\varphi_2 = 75^\circ$ plots around $\varphi = 75^\circ$ in various φ_1 angles,

as observed in the figures. The remaining areas in the ODF's shown exhibited little texture elsewhere, confirming that a significant textural representation is indeed present, as is also observed by the high intensity counts in the diffraction patterns in Figure 7.

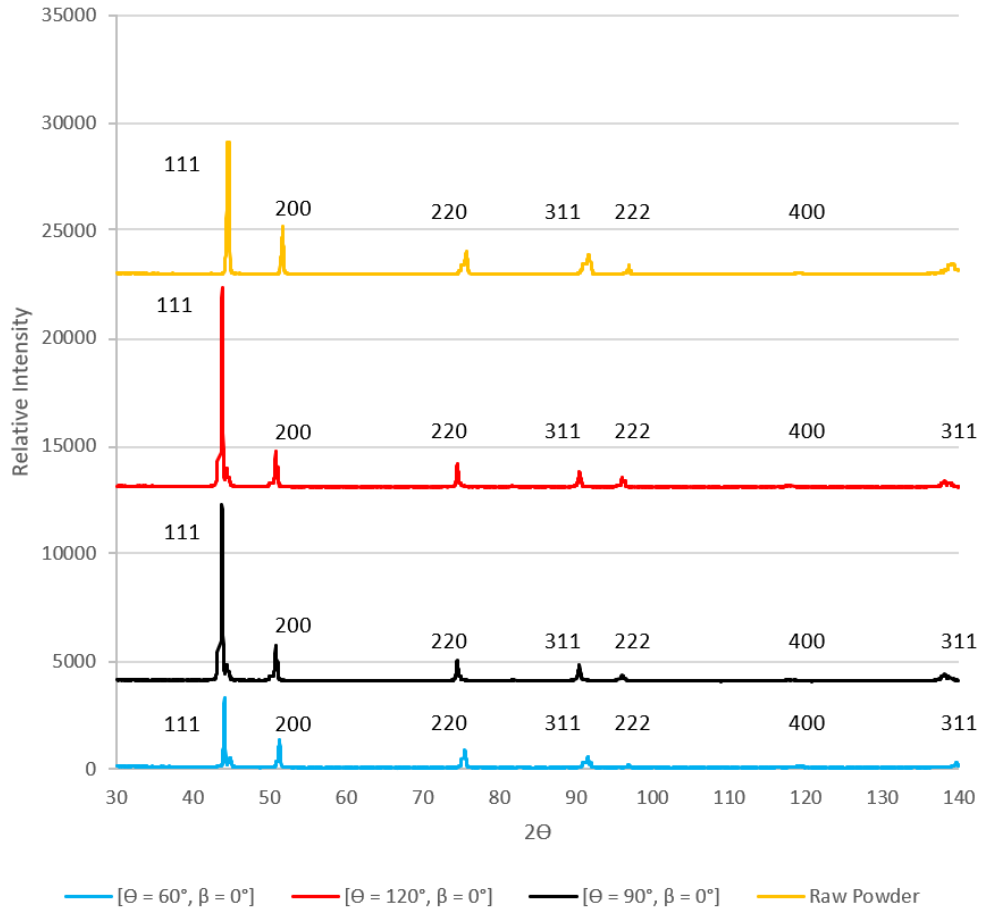


Figure 8. X-Ray diffraction peak patterns. Yellow: raw, unprocessed powder. Red: $\Theta = 120^\circ$ pure lead condition. Black: orthogonal sample. Blue: $\Theta = 60^\circ$ pure lead condition.

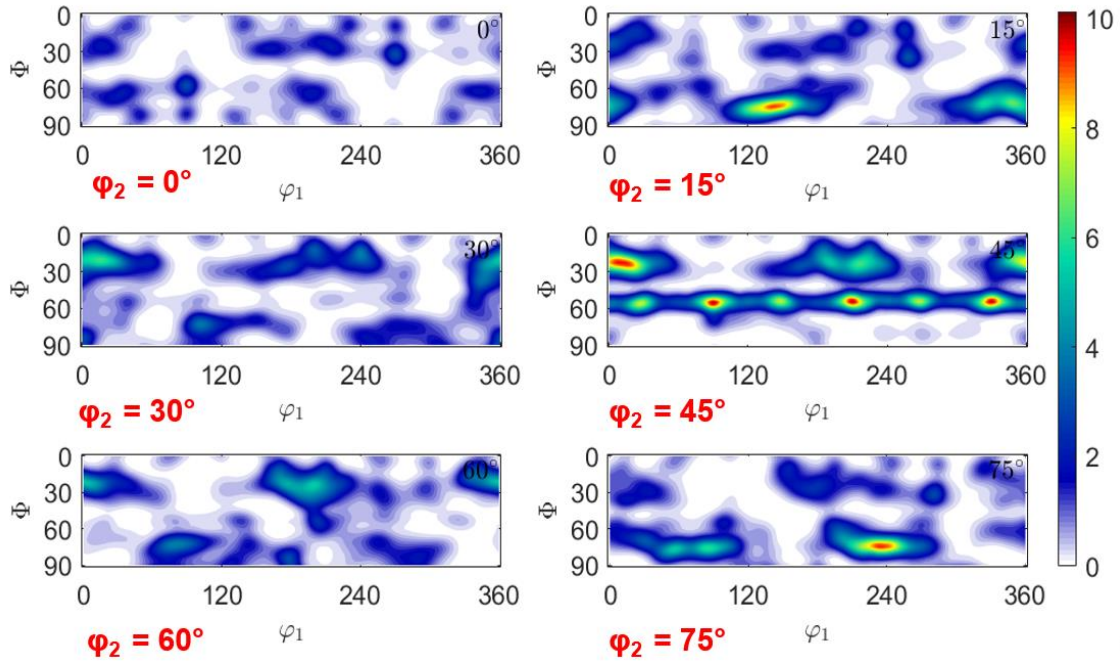


Figure 9. Orientation distribution function plots. $\Theta = 60^\circ$, $\beta = 0^\circ$.

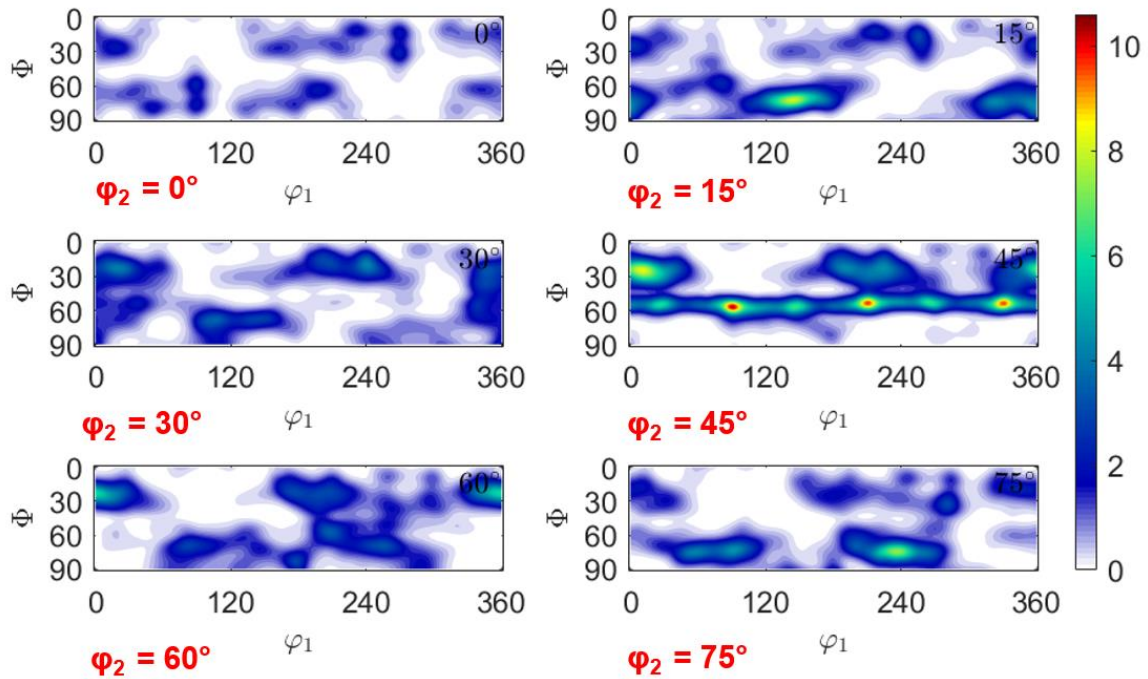


Figure 10. Orientation distribution function plots. $\Theta = 90^\circ$, $\beta = 0^\circ$.

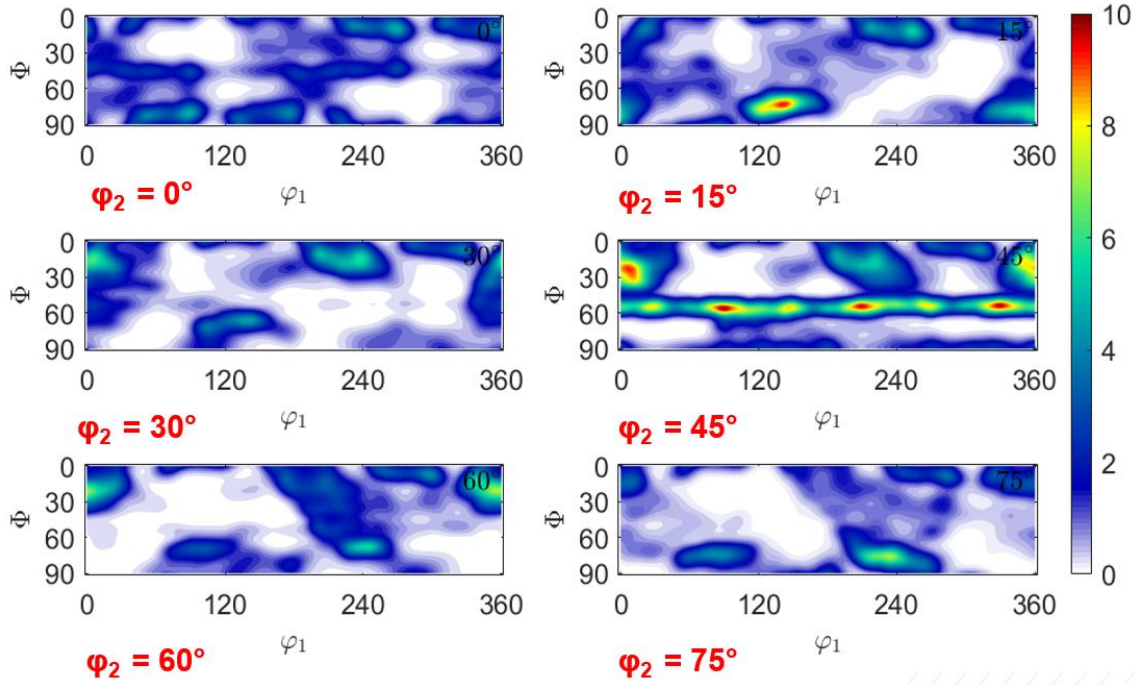


Figure 11. Orientation distribution function plots. $\Theta = 120^\circ$, $\beta = 0^\circ$.

4.1.3 Experiment 3 – Lean & Lead (Pure & Compound) Angle Effects on Bead Microstructure

Figure 12 illustrates the grain size demographics differences of the various regions within a certain sample and across samples for pure lead angle and pure lean/compound angle configurations, respectively. The data was divided into 2 plots: a pure lead condition ($\beta = 0^\circ$) and a compound condition ($\beta = 15^\circ$). Within each plot, all 7 regions that were selected to examine the microstructure are illustrated and are separated from each other as shown. Within each region of the plots, the various angular configurations are situated side-by-side for an easy-to-visualize comparison. This figure setup allows for a more comprehensive view of the grain size within each region, across regions as well as across various angular configurations.

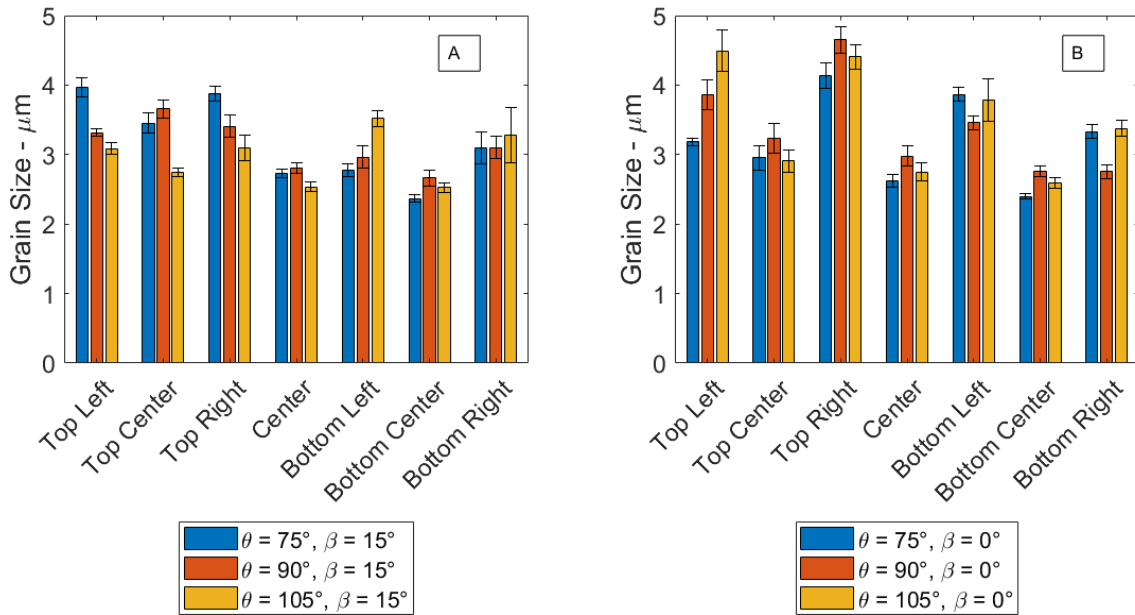


Figure 12. Pure lead, lean and compound angle effects on grain size across samples and sample regions. [A] Pure lean and compound angular configurations. [B] Pure lead and orthogonal angular configurations.

As observed in Figure 12, little microstructure grain size variations were observed with changing lead and lean combinations, across samples, with variations not exceeding 1-1.5 μm . Furthermore, variations between neighboring regions within a sample also did not exceed 2-2.5 μm . Nevertheless, the grains nearest to the center was slightly smaller than on the outer edges of the bead. Figure 13 illustrates the micrographs obtained from pure lean, pure lead, compound and orthogonal angular configurations. Similar solidification fronts were observed in all samples. They all exhibited a radial symmetry which originated in the top center region of the beads, as shown. Columnar and dendritic structures were detected at the outer edges of the bead (more specifically at the bead-substrate interface), while more equiaxed and cellular structures / sub-grains were observed closer to the center of the beads. Appendix B exhibits the micrographs found in Figure 13 at a larger size for the reader's convenience and reference.

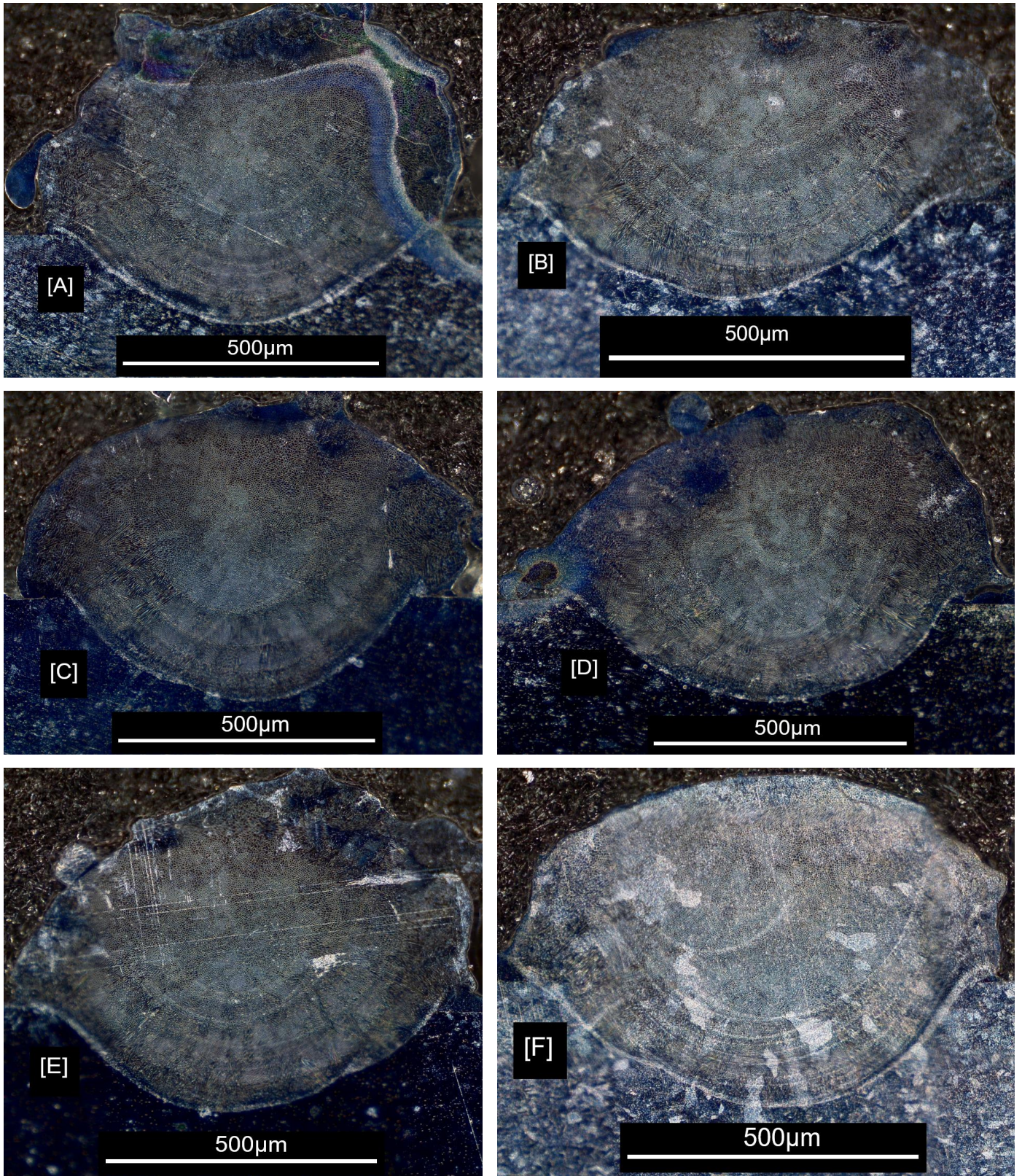


Figure 13. Micrographs of orthogonal and non-orthogonal solidification fronts. A: $\Theta = 75^\circ$, $\beta = 0^\circ$. B: $\Theta = 90^\circ$, $\beta = 0^\circ$. C: $\Theta = 105^\circ$, $\beta = 0^\circ$. D: $\Theta = 75^\circ$, $\beta = 15^\circ$. E: $\Theta = 90^\circ$, $\beta = 15^\circ$. F: $\Theta = 105^\circ$, $\beta = 15^\circ$.

4.1.4 Experiment 4 – Laser Power Attenuation Quantitative Determination Study

Figure 14 illustrates the laser power measurements obtained from this experiment. A drop in power of approximately 25-50W, representing a 6.25% to 12.5% drop from the command power of 400W, was observed when the machine was operated with the powder feed turned off. With regards to the effect of varying the incidence angles, the consequential laser spot size changes that were experienced did not have a specific effect on the amount of power reaching the probe surface. No observable trend was seen in the obtained results, with most data points lying within a 25W range between 350W and 375W. The measured power was, on average, approximately 362.5 ± 12.5 W for all measured incidence angle combinations. When the powder feed was turned on, the measured laser power dropped an additional 25-50W, resulting in a 18.75% to 25% overall drop from the command power of 400W. As also observed when the powder feed was off, changing the laser incidence angle configuration did not have a significant effect on the power measured/absorbed by the probe. The measured power here was, on average, approximately 315 ± 10 W for all measured incidence angle combinations.

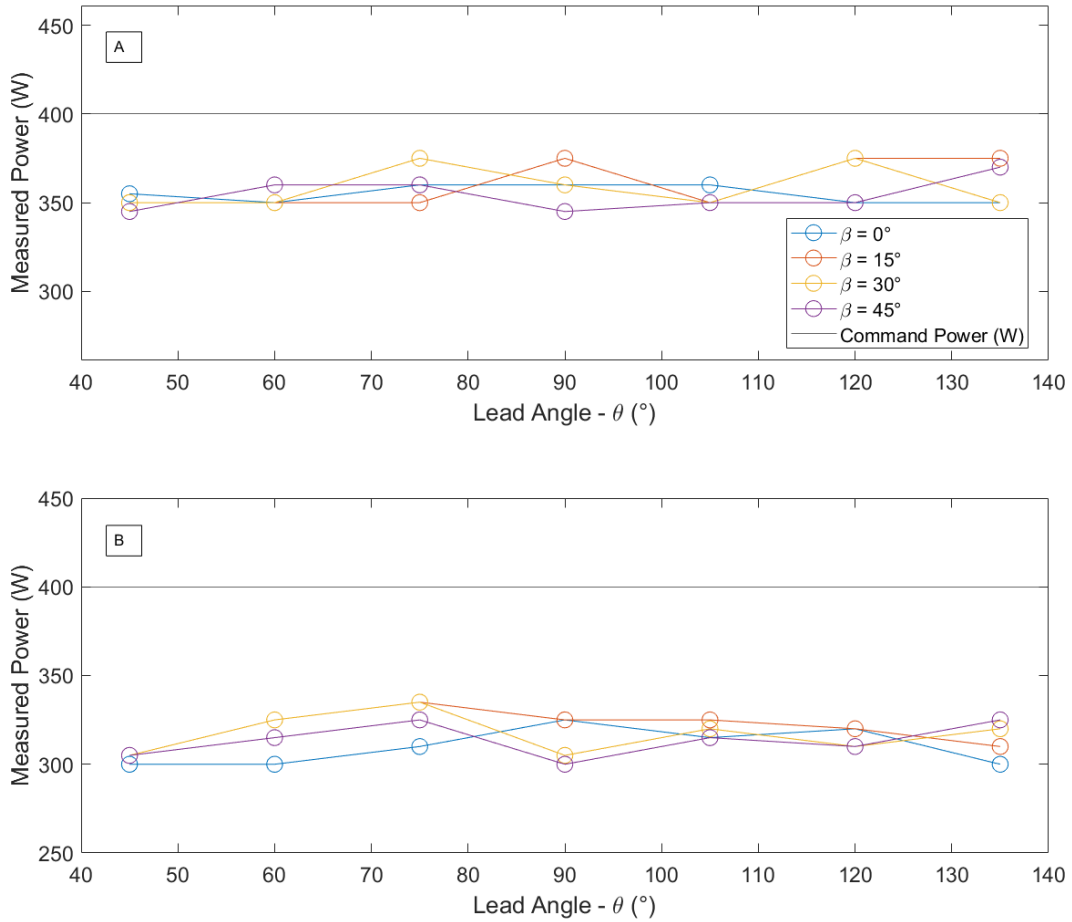


Figure 14. Laser attenuation quantitative measurements. [A] Powder feed turn off. [B] Powder feed turn on.

4.2 Discussion

4.2.1 Experiment 1 - Examination of Laser Incidence Angle Effects on Bead Morphology

In this experiment, it was observed that the bead height, width and penetration depth dropped with increasing lean angles, and followed a normal-type distribution with increasing lead

angles. These results do not match the results obtained by Hao et. al, which show a steady increase in bead width and a somewhat stable bead height with increasing lean angles [16].

With regards to penetration depth, one possible reason why it tends to drop with increasing lead and lean angles is due to the absolute distance travelled by the laser once it interacts with the substrate. In an orthogonal setting, the laser penetrates directly into the thickness of the material, therefore resulting in the highest penetration depth. However, with more inclined lean and lead angles, the laser travel trajectory is now increasingly diagonal to the surface of the substrate. Though it may travel an equivalent absolute distance within the substrate (though at a tilt), the laser in the inclined configuration would result in a smaller absolute penetration depth. Such diminutions in penetration depths have been indeed observed in pulse laser welding of stainless steel, where penetration depth dropped with increasing incidence angles [39]. Figure 15 illustrates that penetration depth drop due to employing non-orthogonal deposition.

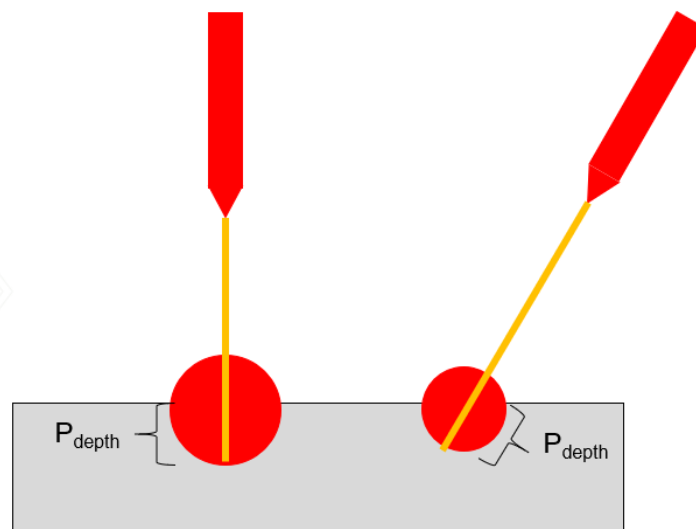


Figure 15. Penetration depth changes due to the employment of non-orthogonal angular configuration.

Given that one of the targets of additive manufacturing is to ensure consistent material properties and geometric characteristics during printing, having a lower penetration depth may be advantageous. With a lower penetration depth, the remelted and recrystallized regions of previously deposited material can be reduced in size, and thus result in a less complex/involved thermal history during the printing process. Thus, the exploitation of non-orthogonal angular configurations can provide some avenues for alternative printing techniques, increasing the robustness of the process.

With regards to bead height and width, it appears that with increasing lean and lead angles, powder catchment becomes an observable issue. As the powder stream exits the coaxial nozzle and begins to interact with the laser, it quickly heats up to melting point and consequently adheres to the melt pool. As the powder stream impacts the substrate surface, not all powder particles within the stream experience full (or even partial) melting. This impartial and/or non-existent melting is a primary reason for the existence of spatter and powder cloud formations, respectively. With such increased incidence angles, the probability of some of the un-melted, partially and fully melted material to leave the melt-pool grows, and is a primary reason for the formation of spatter along the deposit edges [40]. The interaction time between the laser and the powder particles is directly related to the probability of these particles experiencing full, partial or no melting, and this outcome is primarily governed by the distance travelled within the laser's line of action. In other words, the longer a powder particle spends within the laser beam's line of action, the more energy it absorbs, and thus the propensity of it melting increases. Figure 16 illustrates the trajectory of the bounced particles, and how the deposition technique affects powder catchment.

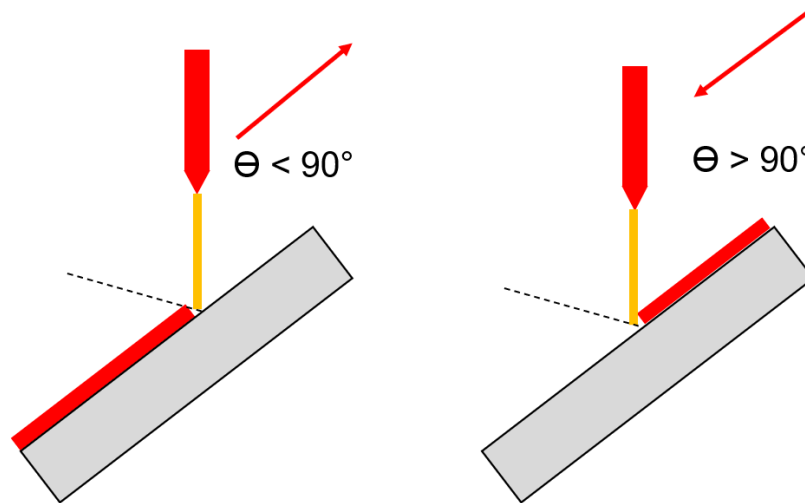


Figure 16. Effect of deposition technique on powder catchment.
The dashed lines represent the bounced particles' trajectory.

During deposition, powder particles hit the melt pool and float momentarily prior to melting [41]. With a continuous flow of powder during deposition, a significant number of powder particles impact those particles that are momentarily suspended in the melt-pool, resulting in bounce-back. In the orthogonal setting, such non-melted powders tend to bounce back at an angle equivalent to the coaxial nozzle geometry, which lies within the 12-15° range. This results in some of these particles to remain within the line of action of the laser, therefore experiencing more heating and subsequent melting in the form of spatter or re-incorporation into the melt-pool. The probability of a powder particle to become part of the spatter or melt-pool demographic is directly dependent on the complex mid-air interactions between powder particles being deposited. Given that the overall trajectory of powder particles in this setting is designed in such a way to ensure adequate powder catchment efficiency is achieved. The coaxial nozzles are also specifically designed to allow for optimum powder catchment when the laser is orthogonal to the substrate surface. However, with higher lean and lead angles, the bounce-back angle of these un-melted

particles increases significantly, thus reducing the interaction time between the laser and such particles. As a result, powder catchment efficiency drops, leading to diminished bead morphology characteristics.

The apparent asymmetry in bead characteristics between lead angles above and below 90° can be attributed to the deposition techniques discussed previously and illustrated in Figures 3 and 16. For lead angles under 90° , as shown, as the particles ricochet off the substrate, they are meant with a 'barrier' of the previously deposited material. As a result, some of the ricochet particles are brought back into the melt-pool, slightly enhancing powder catchment efficiency. However, this phenomenon diminishes with increasingly non-orthogonal angles. For lead angles over 90° , the particles ricochet off the substrate with no previously deposited material to serve as a barrier, therefore resulting in more pronounced decrease in powder catchment efficiency. Figure 16 illustrates this phenomenon.

Another possibility to the asymmetry here could also be due to the difference in the laser beam interactions at and near the melt pool. As the laser beam hits the substrate surface, most of the energy is absorbed by the substrate, while the remainder of the laser energy is reflected. For lead angles under 90° , as the laser beam hits the surface, the reflected energy is met with the previously deposited material. This allows some of that energy to be absorbed by the substrate and the previously deposited material at the tail end of the melt zone as it travels up the substrate. As a result, more energy is deposited into the melt zone, thus allowing for more powder particles to melt. On the other hand, with lead angles larger than 90° , there is no previously deposited material to help concentrate that initially reflected energy, thus resulting in all the reflected energy to travel away from the substrate, hence reducing powder catchment.

In conclusion, it can be conjectured that penetration depth decreases with increasing lead and lean angles due to the diminished absolute distance travelled perpendicularly to the substrate surface. However, the actual laser penetration depth, though at an angle, may be equivalent to the orthogonal configuration. It was also determined that bead height and width decreased possibly due to the reduced laser-powder interaction time experienced as well as the differences in melt-zone characteristics (in terms of reflected laser energy). In an effort to utilize the observed phenomena to the benefit of enhancing the robustness of the process, a couple strategies can be devised. First, the powder feed rate can be increased to accommodate for the powder lost due to the diminished interaction times experienced by the laser at non-orthogonal configurations. This will allow for the bead height and width to increase and thus reach comparable values as the orthogonal setting, while maintaining a low penetration depth. The drawback, however, to this strategy is the increase in material waste during printing. The second strategy can involve increasing the laser power to allow for the limited interaction times experienced to be enough to melt the powders, therefore increasing bead height and width. However, this will result in an increased penetration depth, which makes the thermal history of previously deposited material more complex. A trade-off can be observed in this scenario between increased material waste vs. increased penetration depth, which may yield higher anisotropic behaviors.

4.2.2 *Experiment 2 - Lead Angle Effects on Phase & Texture*

Austenitic FCC phases were observed in both processed and unprocessed samples, as expected. However, no other phases were detected in this experiment, as compared to the detected delta ferrite in Costello et. al.'s efforts [28]. With Cr content slightly under 18 wt%, the Mn content here (~1 wt%) acts as an austenite stabilizer (as compared to becoming a ferrite stabilizer at concentrations around 5-8 wt%) [42]. Furthermore, the presence of Ni in high concentrations

(~13%) also promotes austenite stabilization. Thus, the presence of austenitic FCC phases is valid in this experiment.

The diffraction peak patterns measured for the unprocessed and processed samples nevertheless provide valuable information of the material. The relatively large intensity counts observed for the first (and possibly second) peaks indicate that there is a significant textural representation in the material, even in the case of the unprocessed material, with a substantial intensity count for the 111 crystal plane. The diffraction patterns of all 4 samples were observed to be equivalent, with some slight variations in peak locations and intensities.

The slight differences in diffraction patterns between the unprocessed and processed materials can stem from two possibilities. First, during processing, carbide and/or precipitate formations (which are common in 316L austenitic stainless steels, especially $M_{23}C_6$ carbides) could have occurred during the heating and re-heating of the material as one track is deposited next to the other to form the single layer [43]. The fact that the powder particles are also sized at 44-106 μm , while the recommended powder size for such an experiment is under 500nm, can be a contributor. Slight peak broadening was also observed, which can be attributed to the presence of residual stress (typically observed in additively manufactured materials) as well as the texture representation within the material.

The orientation distribution function results show that a clearly visible fiber texture is present in the processed samples. Specifically, the fiber texture can be seen with consistently high intensities at $\varphi = 60^\circ$, $\varphi_2 = 45^\circ$ and all φ_1 values. This can represent the columnar and dendritic formations that are endemic of the rapid solidification phenomena observed in this process. Some visible texture with high intensities is also present in the $\varphi_2 = 15^\circ$ and $\varphi_2 = 75^\circ$ plots. These can

represent the remainder equiaxed and cellular grain and sub-grain orientations that represent the general microstructural demographic of AM samples. Epitaxial growth can explain the reason behind the heavily fibrous texture representation observed in this process and has been indeed observed in additively manufactured materials [44]. With the very thin layer depositions experienced in DED deposition (around 500 μ m in height, at most), epitaxial phenomena can indeed play a role in the textured nature of AM processed materials.

4.2.3 Experiment 3 - Lean & Lead (Pure & Compound) Angle Effects on Bead Microstructure

The bead microstructure of the various angular configurations examined in this experiment appeared to be equivalent both when comparing regions within a sample and comparing between samples. Similar solidification fronts (directed radially outwards from the center, namely towards the bead-substrate interface) were observed in all samples. Grain size did not change significantly as well. Nevertheless, center regions showed slightly smaller grain size as compared to the outer regions. This can possibly be due to slightly elevated solidification rates as the heat transfer is directed radially outwards towards the substrate. Columnar and some dendritic structure were observed at the bead-substrate interface, while more equiaxed and cellular structures were observed closer to the center. Such solidification microstructure is a common observance in DED-processed materials [45]

The fact that little differences were observed between samples indicates that the solidification phenomena present here are similar, if not equivalent to a degree. This is a fortunate finding, since the ultimate goal of enhancing the process' performance is to increase robustness. With a non-changing microstructure with various angular configurations (while maintaining identical process parameters), a freedom of motion in terms of deposition can be investigated.

More specifically, an opportunity reveals itself in the sense that a transcendence from the conventional 3+2 axis to a 5-axis configuration in the additive portion of this hybrid manufacturing technique is potentially possible from a microstructural standpoint.

4.2.4 *Experiment 4 - Laser Power Attenuation Quantitative Determination Study*

In this experiment, it was observed that laser power experiences losses between 25W-50W with the powder feed turned off, and 75W-100W with the powder feed turned on, providing a clue that laser attenuation does indeed play a detrimental role in laser absorption by the substrate (which, in this case, is the laser power probe). Given that the standoff distance was 33mm for this experiment (to prevent equipment damage), neither the laser beam nor the powder stream were in focus, and thus did not provide an up-close representation of the actual laser-matter interactions in regular deposition operations, where the beam and powder streams are focused. These results match those obtained by Lin et. al [32], where non-focused beams tend to experience less pronounced power losses as compared to focused beams, which can experience up to 50% losses. Given that the experienced power losses with the powder feed on were up to 25%, the results seem reasonable.

Despite the inability of the experimental setup used to accurately describe the laser-matter interactions that typically occur in normal circumstances with focused beams, the goal here was to nonetheless examine relative differences in laser absorption when laser incidence angles are varied. In that respect, the experiment was successful in providing useful information to better understand the effects of incidence angle on laser absorption.

With the powder feed turned off, the experienced power loss of 25-50W can be attributed to the presence of various particulates present within the machine during this operation (i.e.

humidity from machine coolant evaporation, some residual powder particles that remain from previous machine runs...etc...), which cannot be entirely removed from the machine and would be impractical to do so in regular operations. Only in a high vacuum would no power loss be experienced.

The varying of laser incidence angle did not result in an observable trend in laser power loss across all angles with the powder feed turned off. Despite the laser spot size having experienced significant changes (especially at a 33mm standoff distance), the utilized laser power probe only measured the cumulative absorbed power during the 21s exposure time. Within the 21s exposure time, thus, no differences in cumulative absorbed power were observed. Similarly, running the machine with the powder feed on did not result in any observable trends with varying laser incidence angles.

This indicates that more detailed examinations are warranted with more highly capable equipment. Digital power probes with real-time data acquisition capabilities may provide a better idea on the rate of power absorption during the allotted exposure time, which may provide further clues and a more in-depth view of the observed phenomena here.

CHAPTER 5. STUDY LIMITATIONS

As is customary with any work, this study does have limitations that confine its scope. Nevertheless, within the scope of the work conducted here, the experiments were successful in obtaining insightful results that can be used for subsequent studies and applications.

First, with regards to the bead geometry experiment, the absence of advanced process monitoring techniques, such as thermal melt-pool imaging and video capture, does lead to some limitations regarding the conclusions that were made in this study. In other words, in order to prove what was discussed here, it is important to conduct more advanced, in-situ process monitoring, possibly with high speed video capture, to provide an up-close depiction of the actual laser-powder-substrate interactions at play. From there, more confidence can be emphasized on the resultant conclusions from this study. Nevertheless, the results obtained and provided explanations provide an adequate pre-cursor to subsequent studies that are indeed warranted.

With regards to the phase and texture analyses, the slight differences in diffraction patterns between the unprocessed and processed materials can stem from the fact that diffraction experiments are optimum when utilizing particles smaller than 500nm. With bulk materials, some limitations are expected in the overall accuracy. In order to produce the most accurate results, the samples would have needed to be separated from the substrate and ground down to 500nm, which is impractical to do for the scope of this study. Nevertheless, the results obtained were adequate in providing us with the necessary information to move forward with our analyses. Since textural analysis is affected by the overall flatness of the samples, any slight deviations during installation can lead to some inaccuracies to form, which is expected to a degree.

In the microstructural analysis conducted, despite the fact that the manual intercept method only provides a somewhat low-resolution depiction of the microstructure and grain size in general, the goal was to nevertheless examine the relative differences between varying angular configurations. Given that there were no observable differences between them, no further investigation was necessarily required, nor was there a need for more advanced data analysis techniques (i.e. grain size calculator automated algorithm).

In the laser power quantitative measurement, neither the laser beam nor the powder stream was in focus, and thus did not emulate regular deposition operations, where the beam and powder streams are focused. These results match those obtained by Lin et. al [32], where non-focused beams tend to experience less pronounced power losses as compared to focused beams, which can result in up to 50% losses. Despite the inability of the utilized probe to measure laser-matter interactions in focused beams, the goal was to nonetheless examine relative differences in overall laser absorption when laser incidence angles are varied which, in that respect, the experiment was successful in. This indicates that more involved investigations with more capable equipment are warranted to provide a better idea of focused beam laser-matter interactions.

CHAPTER 6. STUDY CONCLUSIONS

In this study, the effects of laser incidence angle on bead morphology, phase composition, textural representation, bead microstructure and resultant power losses were examined. The following conclusions were resultant:

1. The ricochet effect, extent of absorbed reflected energy and resultant powder catchment efficiency play an integral role in bead geometry generation. Acute lead angles are preferred due to the presence of the previously deposited material, which acts as a barrier to ricochet particles and thus enhance powder catchment.
 - a. Bead heights experienced up to 27% and 63% drops in extreme acute and obtuse lead angles, respectively, when compared with the orthogonal condition.
 - b. Bead widths experienced up to 14% and 46% drops in extreme acute and obtuse lead angles, respectively, when compared with the orthogonal condition.
 - c. Penetration depths experienced up to 65% and 89% drops in extreme acute and obtuse lead angles, respectively, when compared with the orthogonal condition.
2. Bead characteristics also dropped with exceedingly non-orthogonal lean angles, though not as significantly as those experienced by lead angles (up to 49%, 27% and 8% drops in penetration depth, bead height and bead width for exceedingly non-orthogonal lean angles).
3. Austenitic FCC phases were observed in both unprocessed powders and the processed samples, with diffraction patterns exhibiting potential texture in the 111 and 200 planes, and some peak broadening representative of residual stress presence in the samples. Little differences between the samples were observed, though.

4. Significant fibrous and other localized textures were present, indicating the presence of columnar/dendritic and equiaxed/cellular structures, respectively. Little textural differences between samples were observed.
5. No significant differences in microstructural composition or grain size were detected with varying incidence angles. Equivalent solidification microstructure was observed, with grain size variations remaining within the 1-1.5 μm and 2-2.5 μm ranges both within and across beads, respectively.
6. Powder feed results in more pronounced laser attenuation when compared to pure laser exposure, with a 75-100W drop from a 400W command power as compared to a 25-50W drop, respectively, for unfocused beams.
7. Laser incidence angle variations do not affect power attenuation for unfocused beams, thus implying that more involved experimentation is required to analyze focused beam laser attenuation behavior with varying angular configurations.

CHAPTER 7. CONTRIBUTION & IMPLICATION OF STUDY FINDINGS

One of the main tenants of a robust manufacturing process is ensuring that consistent material properties and geometric characteristics are maintained in spite of variations in setup configurations. This can be achieved by development a good understanding of the role of process parameters in ensuring robustness is maintained. In this study, the effects of non-orthogonal angular configurations on bead morphology, microstructure, phase composition, texture and absorbed power were examined. Through the experiments conducted, important contributions were made to understanding the underlying phenomena, as well determining possible avenues to enhanced process robustness. More specifically, the main contributions attributed to the work conducted in this study are as follows:

1. Developing an understanding of how bead morphology behaves with increasing lead and lean angles provided an insight on what strategies can be devised to ultimately obtain consistent bead morphologies, regardless of the angular configurations implemented. It also provided insight on the observable trade-offs that must be accounted for when such alternative deposition techniques are used.
2. Observing equivalent phase composition, microstructure and textural representation provides an indication that alternative deposition techniques can be implemented without affecting bulk material properties.
3. Concluding that laser power losses are equivalent with various angular configurations in non-focused beams highlights the importance and urgency of more involved experimentation and analysis in order to truly and fully understand the underlying

phenomena regarding laser power loss due to laser spot size changes and powder cloud laser attenuation.

Though the road to making such alternative deposition techniques industrially implementable is still long, the work conducted in these experiments provided a lot of clues with regards to what would be the logical next steps moving forward.

CHAPTER 8. FUTURE WORK & NEXT STEPS

The results obtained in this study provided valuable insight as to the underlying phenomena at play with regards to non-orthogonal deposition operations. In order to build upon the knowledge gained in this study, a few recommended potential studies can be conducted to bring the non-orthogonal deposition techniques closer to becoming industrially implementable, therefore rendering the hybrid manufacturing process a more robust, and thus more favorable manufacturing technique:

1. Modify process parameters (namely laser power and powder feed rate) to determine what parameters result in consistent bead morphologies for various angular configurations, with the goal being to maximize bead height and width and minimize penetration depth.
2. Examine the effect of multi-track and multi-layer depositions on bead morphology and microstructure of non-orthogonal vs. orthogonal configurations to develop a better understanding of the robustness of the process. This can be done with identical process parameters, or with modified parameters to allow for consistent bead morphologies.
3. Examine the economic implications of non-orthogonal deposition techniques in terms of material waste, cumulative power utilization and printing lead time.
4. Study the effect of utilizing multiple and/or continuously changing angular configurations in multi-track deposition trials on bead morphology and microstructure to examine the simulated effect of deposition on freeform surfaces.

5. Develop theoretical and simulation models, combined with in-situ process monitoring capabilities currently present, to examine the effect of non-orthogonal configurations on powder catchment efficiency, laser attenuation and resultant bead morphology.
6. Develop experimental setups that would allow for accurate laser power measurements of focused beams to obtain a more in-depth view of laser attenuation on printing performance and its effect on bead morphology.
7. Develop novel coaxial nozzle designs that are optimized for non-orthogonal deposition operations and allow for 5-axis deposition, therefore increasing the robustness of the process.

Hybrid manufacturing has an outstanding potential to becoming a viable manufacturing and repair technique to be widely used in industry. By increasing process robustness and developing a more well-rounded and holistic understanding of the phenomena at play, this manufacturing process can manifest to its full potential, thus bringing human progress forward, and ultimately benefitting the environment and society at large.

APPENDIX A. DETAILED MACHINE PARAMETERS

Table A1. XRD Phase Analysis Measurement Parameters (Unprocessed and Processed Samples)

Component	Value
Diffractometer Type	Panalytical Empyrean
Processed Sample Configuration	Chi-Phi-Z Stage
Unprocessed Sample Configuration	Reflection-Transmission Spinner
Goniometer Type	Theta/Theta
Minimum 2Θ Step Size ($^{\circ}$)	0.0001
Minimum Ω Step Size ($^{\circ}$)	0.0001
Minimum Chi Step Size ($^{\circ}$)	0.01
Minimum Phi Step Size ($^{\circ}$)	0.01
Minimum z Step Size (mm)	0.001
Reflection Height (mm)	240
Anode Material	Cu
K- α_1 Wavelength (\AA)	1.540598
K- α_2 Wavelength (\AA)	1.544426
K- α_1 - K- α_2 Ratio	0.5
Divergence Slit (mm)	0.38 (Fixed)
Unprocessed Sample Divergence Slit (mm)	0.05 (Fixed)
Monochromator Usage	No
Generator Voltage (kV)	45
Tube Current (mA)	40
Scan Axis	Gonio
Scan Type	Continuous
Scan Range ($^{\circ}$)	29.9945 – 140
Scan Step Size ($^{\circ}$)	0.026261
Time per Step (s)	197.115

APPENDIX B. MICROGRAPH CLOSE-UPS

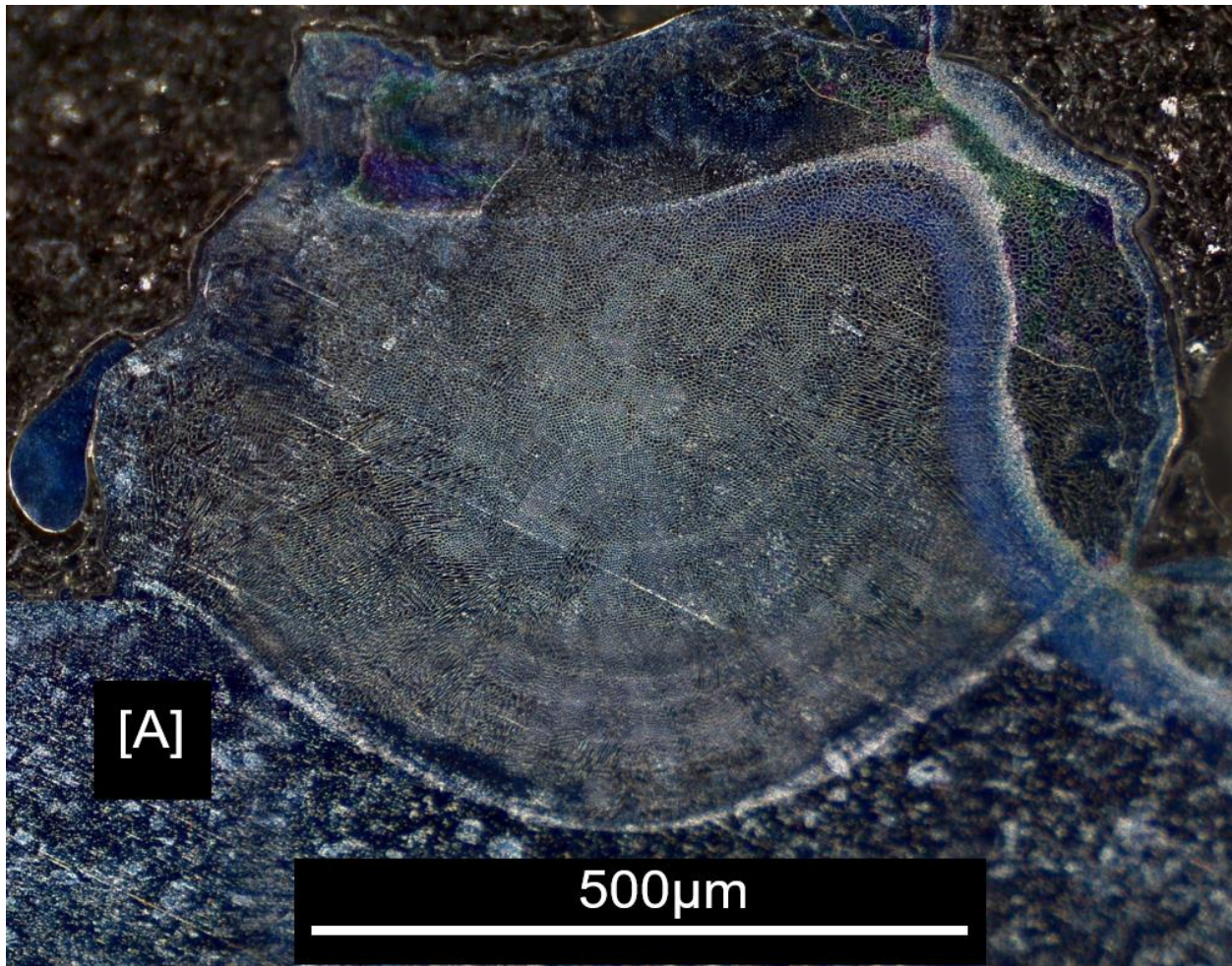


Figure B1. Micrograph close-up. A: $\Theta = 75^\circ$, $\beta = 0^\circ$.

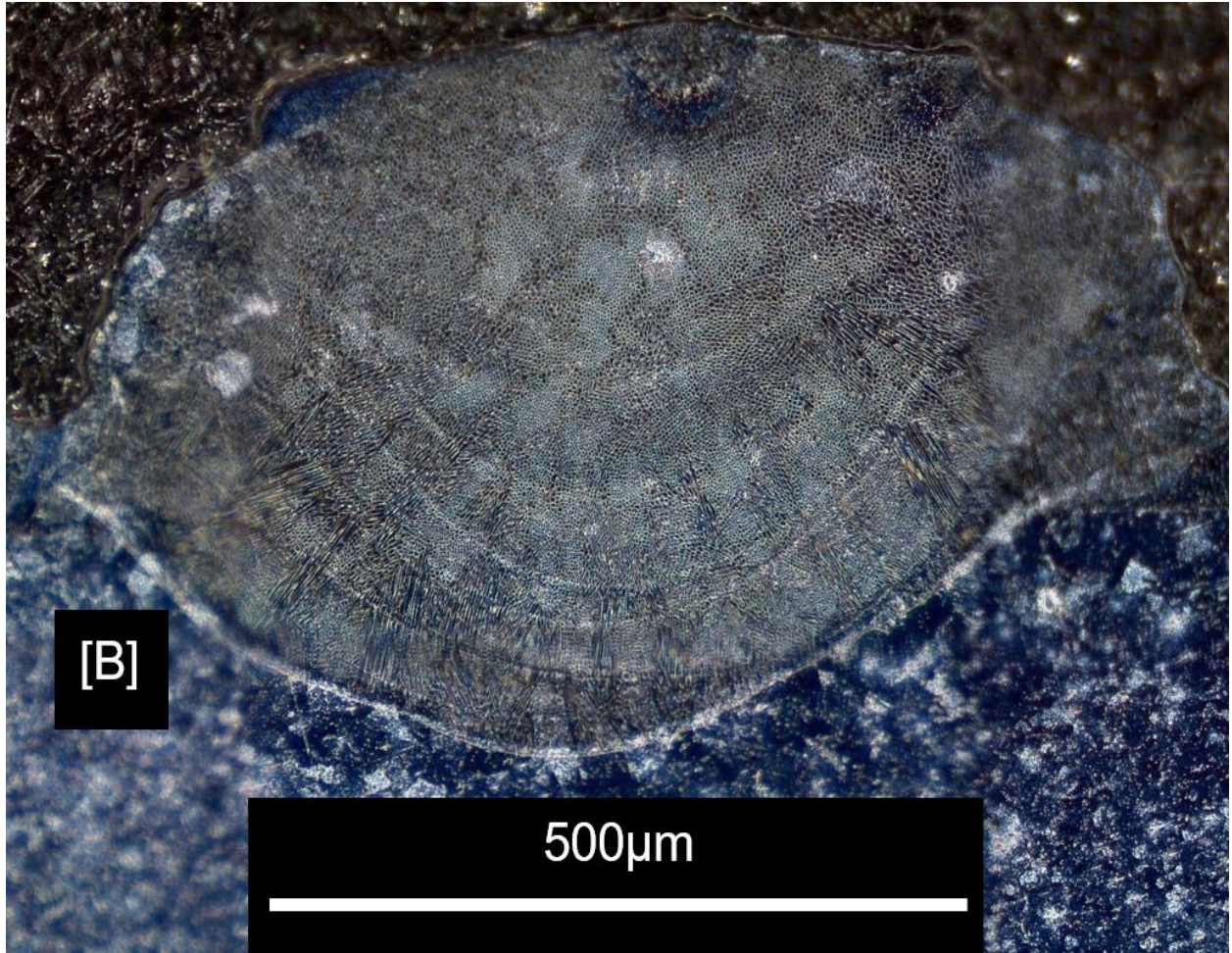


Figure B2. Micrograph close-up. B: $\Theta = 90^\circ$, $\beta = 0^\circ$.

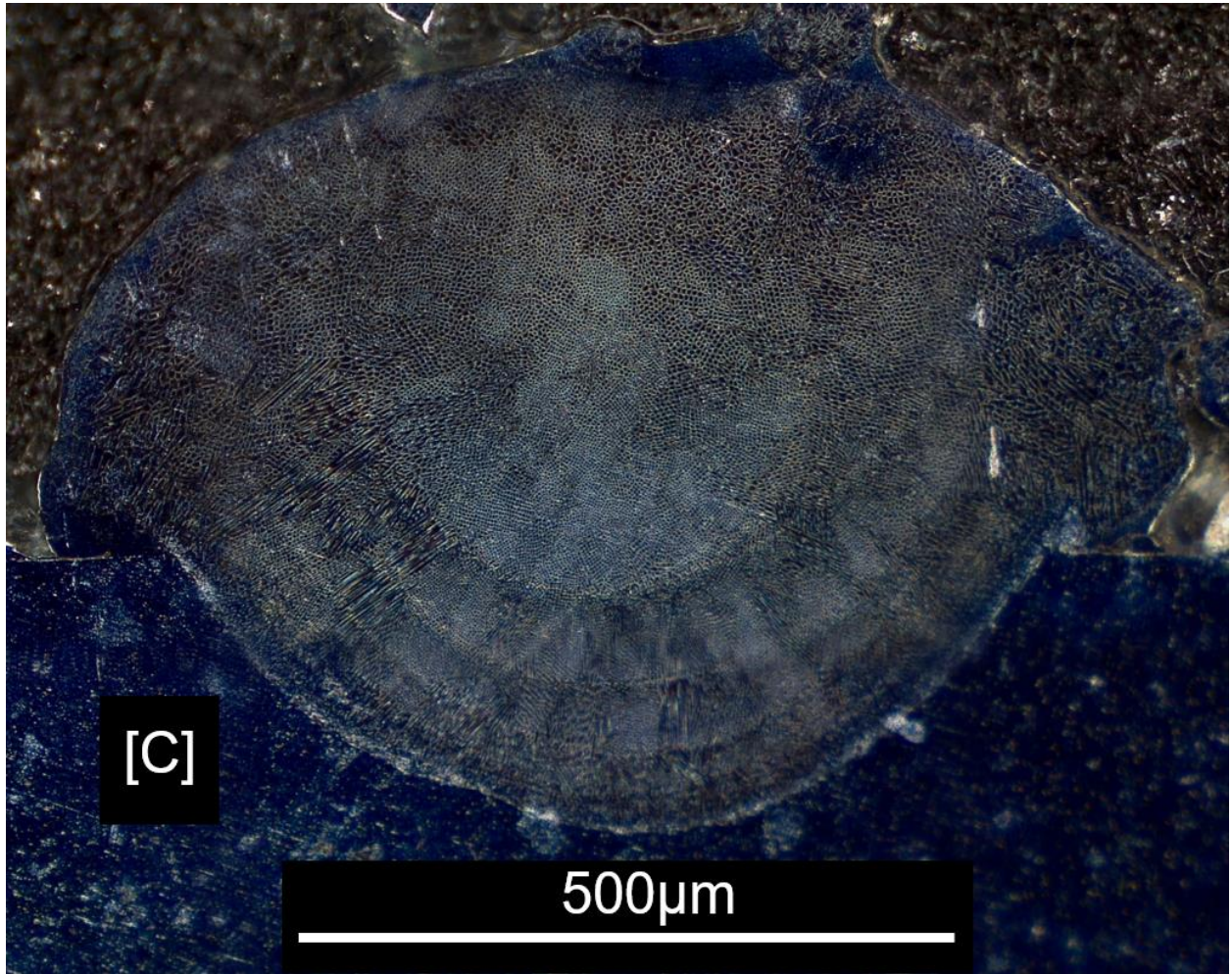


Figure B3. Micrograph close-up. C: $\Theta = 105^\circ$, $\beta = 0^\circ$.

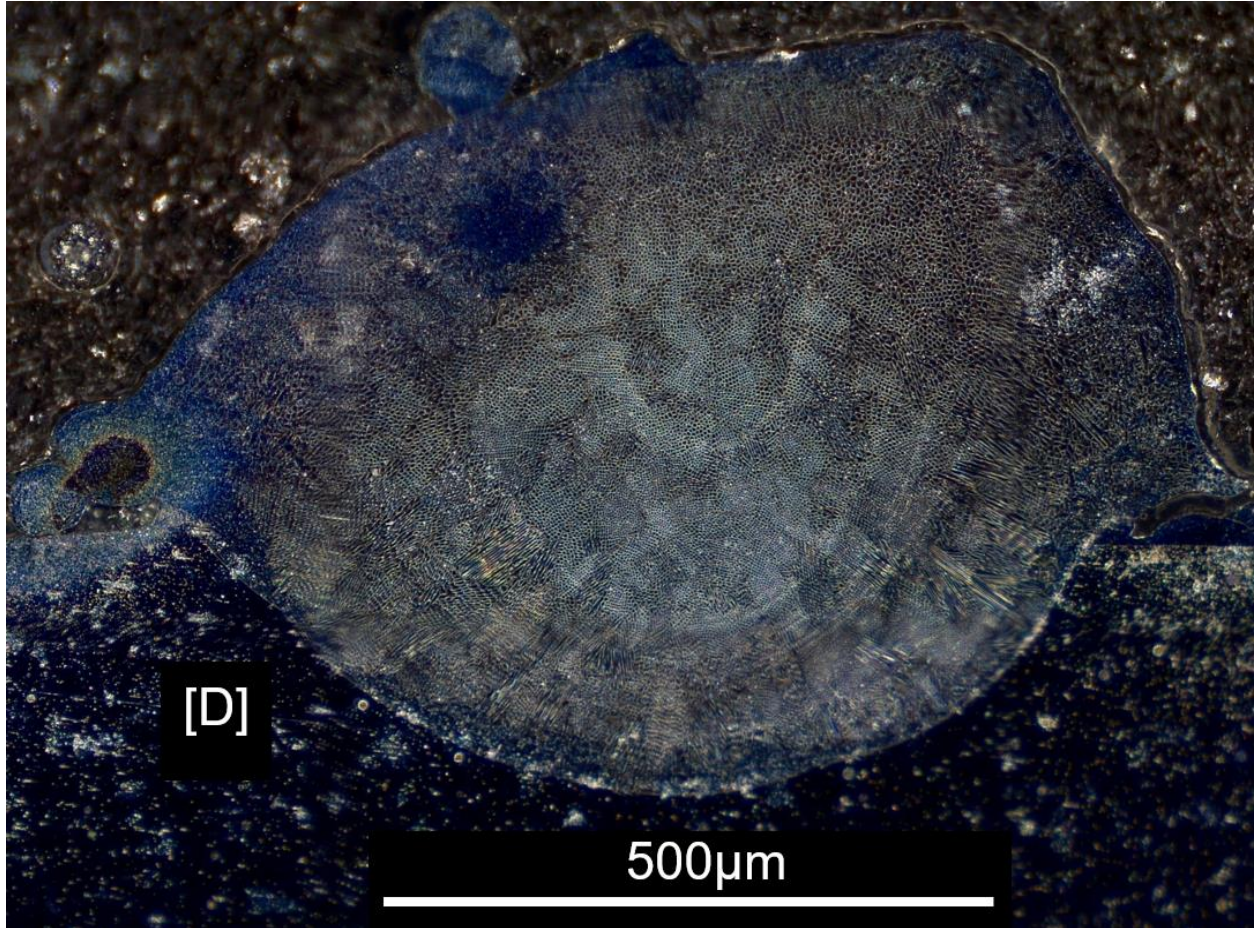


Figure B4. Micrograph close-up. D: $\Theta = 75^\circ$, $\beta = 15^\circ$.

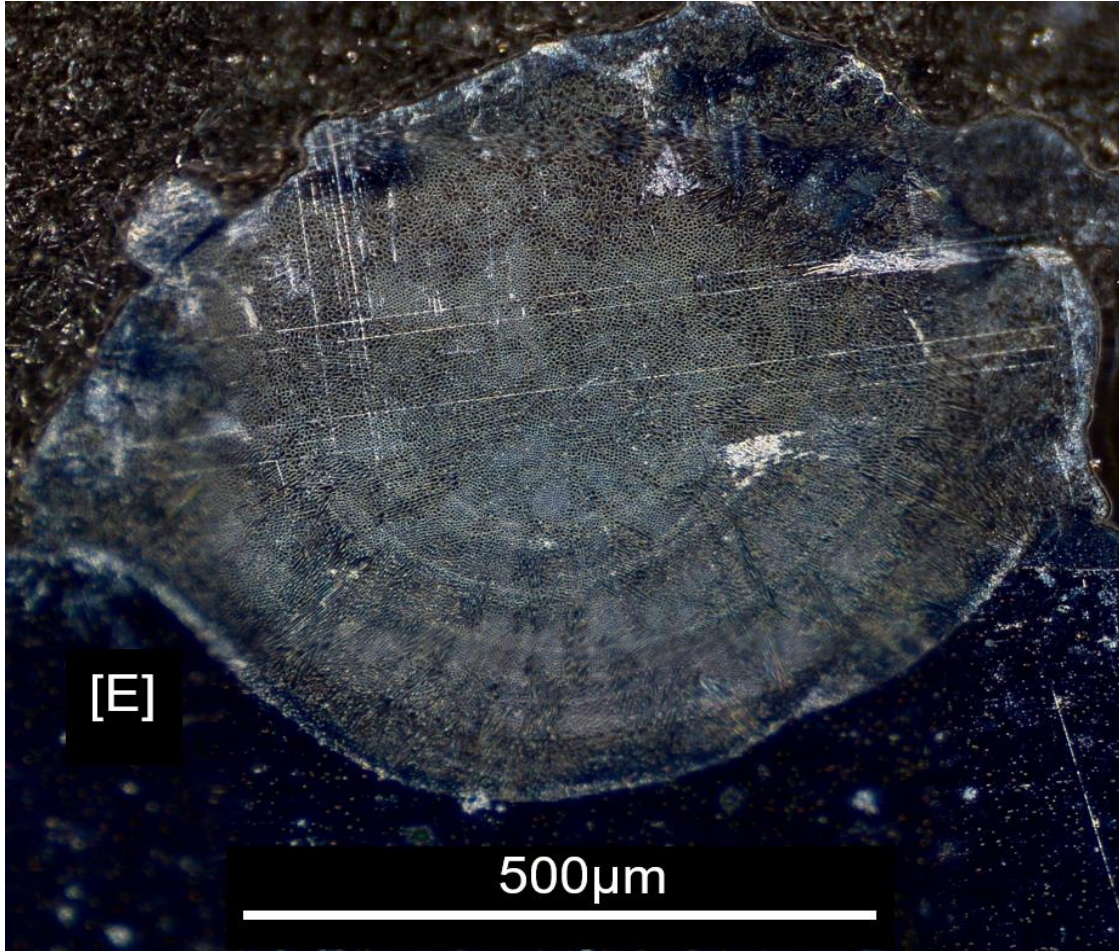


Figure B5. Micrograph close-up. E: $\Theta = 90^\circ$, $\beta = 15^\circ$.

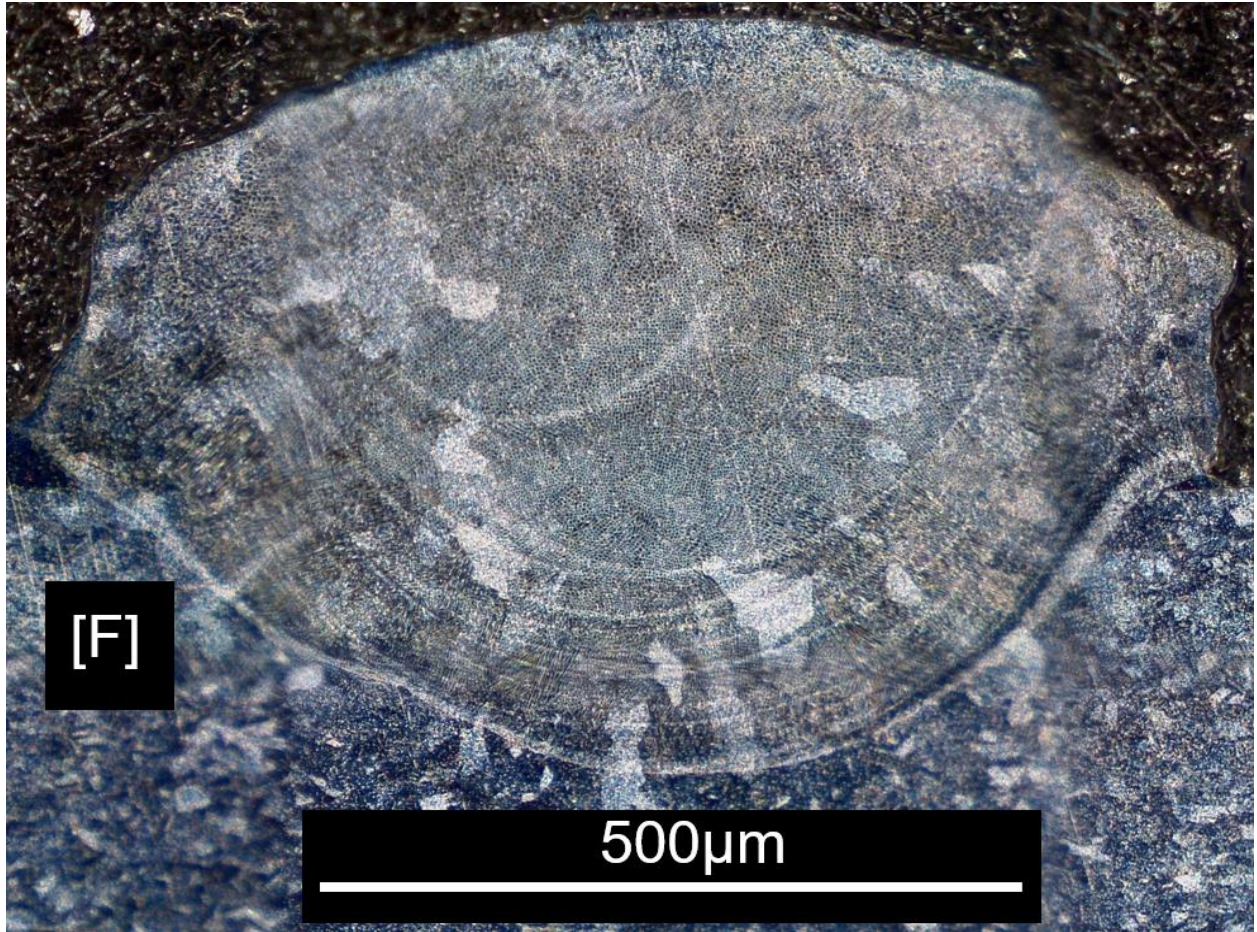


Figure B6. Micrograph close-up. B: $\Theta = 105^\circ$, $\beta = 15^\circ$.

REFERENCES

- [1] Zhu, Z., V. G. Dhokia, A. Nassehi, and S. T. Newman. "A Review of Hybrid Manufacturing Processes – State of the Art and Future Perspectives." *International Journal of Computer Integrated Manufacturing* 26, no. 7 (July 1, 2013): 596–615. <https://doi.org/10.1080/0951192X.2012.749530>
- [2] Wilson, J. Michael, Cecil Piya, Yung C. Shin, Fu Zhao, and Karthik Ramani. "Remanufacturing of Turbine Blades by Laser Direct Deposition with Its Energy and Environmental Impact Analysis." *Journal of Cleaner Production* 80 (October 1, 2014): 170–78. <https://doi.org/10.1016/j.jclepro.2014.05.084>
- [3] Elser, Anja, Michael Königs, Alexander Verl, and Michael Servos. "On Achieving Accuracy and Efficiency in Additive Manufacturing: Requirements on a Hybrid CAM System." *Procedia CIRP*, 51st CIRP Conference on Manufacturing Systems, 72 (January 1, 2018): 1512–17. <https://doi.org/10.1016/j.procir.2018.03.265>
- [4] Materialise. "Software Solutions for Data Preparation." Accessed July 16, 2020. <https://www.materialise.com/en/software/software-solutions-for-data-preparation>.
- [5] Jiang, Jingchao, Xun Xu, and Jonathan Stringer. "Support Structures for Additive Manufacturing: A Review." *Journal of Manufacturing and Materials Processing* 2, no. 4 (December 2018): 64. <https://doi.org/10.3390/jmmp2040064>
- [6] Taufik, Mohammad, and Prashant K. Jain. "Role of Build Orientation in Layered Manufacturing: A Review." *International Journal of Manufacturing Technology and Management* 27, no. 1/2/3 (2013): 47. <https://doi.org/10.1504/IJMTM.2013.058637>
- [7] Kumbhar, N. N., and A. V. Mulay. "Post Processing Methods Used to Improve Surface Finish of Products Which Are Manufactured by Additive Manufacturing Technologies: A Review." *Journal of The Institution of Engineers (India): Series C* 99, no. 4 (August 1, 2018): 481–87. <https://doi.org/10.1007/s40032-016-0340-z>.
- [8] "Committee F42 on Additive Manufacturing Technologies - Published Standards under F42 Jurisdiction." Accessed July 16, 2020. <https://www.astm.org/COMMIT/SUBCOMMIT/F42.htm>.
- [9] "Additive Manufacturing | CAM Software | OPEN MIND." Accessed July 16, 2020. <https://www.openmind-tech.com/en-us/cam/additive-manufacturing.html>.
- [10] Lasemi, Ali, Deyi Xue, and Peihua Gu. "Recent Development in CNC Machining of Freeform Surfaces: A State-of-the-Art Review." *Computer-Aided Design* 42, no. 7 (July 1, 2010): 641–54. <https://doi.org/10.1016/j.cad.2010.04.002>
- [11] Najmon, Joel C., Sajjad Raeisi, and Andres Tovar. "2 - Review of Additive Manufacturing Technologies and Applications in the Aerospace Industry." In *Additive Manufacturing for the Aerospace Industry*, edited by Francis Froes and Rodney Boyer, 7–31. Elsevier, 2019. <https://doi.org/10.1016/B978-0-12-814062-8.00002-9>

- [12] “VC-500 AM.” Accessed July 16, 2020. <https://www.mazakusa.com/machines/vc-500-am/>.
- [13] “LASERTEC 65 3D Hybrid - Additive Manufacturing Machines from DMG MORI.” Accessed July 16, 2020. <https://us.dmgmori.com/products/machines/additive-manufacturing/powder-nozzle/lasertec-65-3d-hybrid>.
- [14] Matsuura Machinery USA. “LUMEX Avance-25,” September 5, 2017. <https://www.matsuurausa.com/model/lumex-avance-25/>.
- [15] Leyens, C., and E. Beyer. “8 - Innovations in Laser Cladding and Direct Laser Metal Deposition.” In *Laser Surface Engineering*, edited by J. Lawrence and D. G. Waugh, 181–92. Woodhead Publishing Series in Electronic and Optical Materials. Woodhead Publishing, 2015. <https://doi.org/10.1016/B978-1-78242-074-3.00008-8>.
- [16] Hao, Jingbin, Qingdong Meng, Congcong Li, Zhixiong Li, and Dazhong Wu. “Effects of Tilt Angle between Laser Nozzle and Substrate on Bead Morphology in Multi-Axis Laser Cladding.” *Journal of Manufacturing Processes* 43 (July 2019): 311–22. <https://doi.org/10.1016/j.jmapro.2019.04.025>
- [17] Leung, Chu Lun Alex, Sebastian Marussi, Michael Towrie, Jesus del Val Garcia, Robert C. Atwood, Andrew J. Bodey, Julian R. Jones, Philip J. Withers, and Peter D. Lee. “Laser-Matter Interactions in Additive Manufacturing of Stainless Steel SS316L and 13-93 Bioactive Glass Revealed by in Situ X-Ray Imaging.” *Additive Manufacturing* 24 (December 1, 2018): 647–57. <https://doi.org/10.1016/j.addma.2018.08.025>
- [18] H. L. Wei, J. Mazumder, T. DebRoy, “Evolution of Solidification Texture during Additive Manufacturing | Scientific Reports.”, (14 October 2015) <https://www.nature.com/articles/srep16446>
- [19] Lewandowski, John J., and Mohsen Seifi. “Metal Additive Manufacturing: A Review of Mechanical Properties.” *Annual Review of Materials Research* 46, no. 1 (2016): 151–86. <https://doi.org/10.1146/annurev-matsci-070115-032024>
- [20] Strondl, A., O. Lyckfeldt, H. Brodin, and U. Ackelid. “Characterization and Control of Powder Properties for Additive Manufacturing.” *JOM* 67, no. 3 (March 1, 2015): 549–54. <https://doi.org/10.1007/s11837-015-1304-0>
- [21] Kakinuma, Yasuhiro, Masahiko Mori, Yohei Oda, Takanori Mori, Makoto Kashihara, Adam Hansel, and Makoto Fujishima. “Influence of Metal Powder Characteristics on Product Quality with Directed Energy Deposition of Inconel 625.” *CIRP Annals* 65, no. 1 (January 1, 2016): 209–12. <https://doi.org/10.1016/j.cirp.2016.04.058>
- [22] Ahsan, M. Naveed, Andrew J. Pinkerton, Richard J. Moat, and Judith Shackleton. “A Comparative Study of Laser Direct Metal Deposition Characteristics Using Gas and Plasma-Atomized Ti–6Al–4V Powders.” *Materials Science and Engineering: A* 528, no. 25 (September 25, 2011): 7648–57. <https://doi.org/10.1016/j.msea.2011.06.074>

- [23] Zhong, Chongliang, Jing Chen, Stefanie Linnenbrink, Andres Gasser, Shang Sui, and Reinhart Poprawe. “A Comparative Study of Inconel 718 Formed by High Deposition Rate Laser Metal Deposition with GA Powder and PREP Powder.” *Materials & Design* 107 (October 5, 2016): 386–92. <https://doi.org/10.1016/j.matdes.2016.06.037>
- [24] Mahmood, Khalid, and Andrew J Pinkerton. “Direct Laser Deposition with Different Types of 316L Steel Particle: A Comparative Study of Final Part Properties.” *Proceedings of the Institution of Mechanical Engineers, Part B: Journal of Engineering Manufacture* 227, no. 4 (April 1, 2013): 520–31. <https://doi.org/10.1177/0954405413475961>
- [25] Lewandowski, John J., and Mohsen Seifi. “Metal Additive Manufacturing: A Review of Mechanical Properties.” *Annual Review of Materials Research* 46, no. 1 (2016): 151–86. <https://doi.org/10.1146/annurev-matsci-070115-032024>
- [26] Collins, P.C., D.A. Brice, P. Samimi, I. Ghamarian, and H.L. Fraser. “Microstructural Control of Additively Manufactured Metallic Materials.” *Annual Review of Materials Research* 46, no. 1 (2016): 63–91. <https://doi.org/10.1146/annurev-matsci-070115-031816>
- [27] Ravi, G. A., Chunlei Qiu, and Moataz M. Attallah. “Microstructural Control in a Ti-Based Alloy by Changing Laser Processing Mode and Power during Direct Laser Deposition.” *Materials Letters* 179 (September 15, 2016): 104–8. <https://doi.org/10.1016/j.matlet.2016.05.038>
- [28] Costello, Aaron C., Santhosh K. Koduri, and James W. Sears. “Optimization of Laser Powder Deposition for 316L Stainless Steel.” *International Congress on Applications of Lasers & Electro-Optics 2003*, no. 1 (October 1, 2003): 701. <https://doi.org/10.2351/1.5060072>
- [29] Kobryn, P. A., E. H. Moore, and S. L. Semiatin. “The Effect of Laser Power and Traverse Speed on Microstructure, Porosity, and Build Height in Laser-Deposited Ti-6Al-4V.” *Scripta Materialia* 43, no. 4 (July 28, 2000): 299–305. [https://doi.org/10.1016/S1359-6462\(00\)00408-5](https://doi.org/10.1016/S1359-6462(00)00408-5)
- [30] Ruiz, Jose Exequiel, Magdalena Cortina, Jon Iñaki Arrizubieta, and Aitzol Lamikiz. “Study of the Influence of Shielding Gases on Laser Metal Deposition of Inconel 718 Superalloy.” *Materials* 11, no. 8 (August 2018): 1388. <https://doi.org/10.3390/ma11081388>
- [31] Eo, Du-Rim, Sun-Hong Park, and Jung-Wook Cho. “Controlling Inclusion Evolution Behavior by Adjusting Flow Rate of Shielding Gas during Direct Energy Deposition of AISI 316 L.” *Additive Manufacturing* 33 (May 1, 2020): 101119. <https://doi.org/10.1016/j.addma.2020.101119>
- [32] Lin, Jehnming. “Laser Attenuation of the Focused Powder Streams in Coaxial Laser Cladding.” *Journal of Laser Applications* 12, no. 1 (January 18, 2000): 28–33. <https://doi.org/10.2351/1.521910>
- [33] Kim, Min-seob, Wook-jin Oh, Gyeong-yoon Baek, Yeong-kwan Jo, Ki-yong Lee, Sang-hu Park, and Do-sik Shim. “Ultrasonic Nanocrystal Surface Modification of High-Speed Tool Steel (AISI M4) Layered via Direct Energy Deposition.” *Journal of Materials Processing Technology* 277 (March 1, 2020): 116420. <https://doi.org/10.1016/j.jmatprotec.2019.116420>

- [34] Grasso, M., A. G. Demir, B. Previtali, and B. M. Colosimo. "In Situ Monitoring of Selective Laser Melting of Zinc Powder via Infrared Imaging of the Process Plume." *Robotics and Computer-Integrated Manufacturing* 49 (February 1, 2018): 229–39. <https://doi.org/10.1016/j.rcim.2017.07.001>
- [35] Fu, Yunchang, A. Loredó, B. Martín, and A. B. Vannes. "A Theoretical Model for Laser and Powder Particles Interaction during Laser Cladding." *Journal of Materials Processing Technology* 128, no. 1 (October 6, 2002): 106–12. [https://doi.org/10.1016/S0924-0136\(02\)00433-8](https://doi.org/10.1016/S0924-0136(02)00433-8)
- [36] Liu, Jichang, Lijun Li, Yuanzhong Zhang, and Xiaozhu Xie. "Attenuation of Laser Power of a Focused Gaussian Beam during Interaction between a Laser and Powder in Coaxial Laser Cladding." *Journal of Physics D: Applied Physics* 38, no. 10 (May 21, 2005): 1546–50. <https://doi.org/10.1088/0022-3727/38/10/008>
- [37] Pinkerton, Andrew J. "An Analytical Model of Beam Attenuation and Powder Heating during Coaxial Laser Direct Metal Deposition." *Journal of Physics D: Applied Physics* 40, no. 23 (November 2007): 7323–7334. <https://doi.org/10.1088/0022-3727/40/23/012>
- [38] Abrams, Halle. "Grain Size Measurement by the Intercept Method." *Metallography* 4, no. 1 (February 1, 1971): 59–78. [https://doi.org/10.1016/0026-0800\(71\)90005-X](https://doi.org/10.1016/0026-0800(71)90005-X)
- [39] Liao, Yi-Chun, and Ming-Huei Yu. "Effects of Laser Beam Energy and Incident Angle on the Pulse Laser Welding of Stainless Steel Thin Sheet." *Journal of Materials Processing Technology* 190, no. 1 (July 23, 2007): 102–8. <https://doi.org/10.1016/j.jmatprotec.2007.03.102>
- [40] Siva Prasad, Himani, Frank Brueckner, and Alexander F. H. Kaplan. "Powder Incorporation and Spatter Formation in High Deposition Rate Blown Powder Directed Energy Deposition." *Additive Manufacturing* 35 (October 1, 2020): 101413. <https://doi.org/10.1016/j.addma.2020.101413>
- [41] Haley, James C., Julie M. Schoenung, and Enrique J. Lavernia. "Observations of Particle-Melt Pool Impact Events in Directed Energy Deposition." *Additive Manufacturing* 22 (August 1, 2018): 368–74. <https://doi.org/10.1016/j.addma.2018.04.028>
- [42] Shuro, I., S. Kobayashi, T. Nakamura, and K. Tsuzaki. "Determination of α/γ Phase Boundaries in the Fe–Cr–Ni–Mn Quaternary System with a Diffusion-Multiple Method." *Journal of Alloys and Compounds* 588 (March 5, 2014): 284–89. <https://doi.org/10.1016/j.jallcom.2013.11.095>
- [43] Lee, J. H., and Y. S. Kim. "Intergranular Corrosion of 316L Stainless Steel by Aging and UNSM (Ultrasonic Nano-crystal Surface Modification) treatment." *Corrosion Science and Technology* 14, no. 6 (2015): 313–24. <https://doi.org/10.14773/cst.2015.14.6.313>
- [44] Basak, Amrita, and Suman Das. "Epitaxy and Microstructure Evolution in Metal Additive Manufacturing." *Annual Review of Materials Research* 46, no. 1 (2016): 125–49. <https://doi.org/10.1146/annurev-matsci-070115-031728>

[45] Saboori, Abdollah, Donato Gallo, Sara Biamino, Paolo Fino, and Mariangela Lombardi. “An Overview of Additive Manufacturing of Titanium Components by Directed Energy Deposition: Microstructure and Mechanical Properties.” *Applied Sciences* 7, no. 9 (September 2017): 883. <https://doi.org/10.3390/app7090883>.